NHRP

Natural Hazards Research Platform

Tsunami Resilience of New Zealand Ports

Final Report

Impact Statement 2

Project: 2012-GNS-03-NHRP

February 2016

Bruce Melville

Asaad Shamseldin

Liam Wotherspoon

Ben Popovich

Cheng Chen

Abstract

Ports are of critical importance to New Zealand. For the year ending in June 2011, the New Zealand government reported that 99% of imports and exports by weight arrived or departed through ports (Statistics NZ, 2012). In addition, ports are a lifeline through which foreign aid and equipment must pass in the event of a natural disaster. Thus it is of the utmost importance that this essential infrastructure withstands such events. Ports' locations along the coast expose them to a variety of potential hazards, one of which is tsunami. Tsunami have historically been destructive to the infrastructure they impact and due to New Zealand's exposed location, tsunami generated by events at any position along the Pacific Rim may impact New Zealand. This research seeks to predict damage to port infrastructure from tsunami loads. Since the assessment of all infrastructure is not possible and the concentration was be on wharves, one of the most fundamental and critical structural types found in ports.

This research was carried out in two main phases. The first involved quantifying tsunami loads from a combination of experimental studies and design standards. Physical experimentation was carried out at the University of Auckland to quantify hydrodynamic uplift loads on wharf structures. The remaining lateral loads were derived from international design standards. The second phase of research involved developing structural wharf models that were representative of existing infrastructure present at New Zealand ports. These models combined many structural, material, and geotechnical characteristics attained from construction drawings and other port documentation. The tsunami loads, representing a range of wave heights, were applied to the structural models in order to examine the resulting damage states to the structures. The result of this research was a series of plots detailing damage states to specific elements within the structural models and a final plot comparing the overall level of damage to the wharf structures versus the impacting tsunami bore height.

Table of Contents

List of Figures

List of Tables

List of Equations

Chapter 1: Introduction

New Zealand is a nation in the southern Pacific Ocean comprising two main large islands and several smaller islands. New Zealand is home to approximately 4.5 million people, the majority of whom live along the nation's vast coastline. The economy in New Zealand comprises mostly agriculture industries and relies heavily on efficiently exporting those goods while importing others. Approximately 99% of all imports and exports entering or leaving New Zealand pass through New Zealand seaports (Statistics NZ, 2012). Most of these goods are serviced by one of the 14 major ports which are spread out over both islands. Thus, these major ports are critically important to the economic function and prosperity of New Zealand. Due to New Zealand's position along the Pacific "Ring of Fire", it is exposed to a variety of natural hazards including earthquakes, volcanoes, and tsunami. While extensive research has been carried out regarding New Zealand's exposure and risk to earthquakes and volcanoes, the literature related to tsunami impact on infrastructure is not as extensive.

A tsunami is a large wave or series of waves that occurs as a result of the displacement of a large volume of water. These displacements may occur as a result of many events including large earthquakes, underwater landslides, coastal landslides, meteorite impacts, or volcanic eruptions. Approximately 90% of all tsunami are caused by large earthquakes (Bormann 2008). Tsunami are distinguishable from normal waves because the disruption affects the entire water column. The energy built up by a tsunami does not dissipate easily as with typical wind-driven waves, allowing tsunami to travel vast, trans-oceanic distances and still attain great wave heights and sustained inundation upon reaching the shore. Upon inundation, the first interaction will be with New Zealand's coastline and coastal infrastructure. As some of this coastal infrastructure, particularly ports, is critical to

New Zealand's successful operation, it is essential to evaluate the risk presented by its inundation from tsunami.

1.1 Goals

The goal of this study is to quantify tsunami loading characteristics ad estimate the damage states of port infrastructure following tsunami impact. Ports encompass an extensive variety of infrastructure types, each of which may be subject to different tsunami related effect. Wharves are critical berthing structures subject to a unique load regime consisting of hydrodynamic uplift and lateral loads during a tsunami as well as extensive scouring of their foundation. Other port infrastructure, such as certain types of semi-solid or solid fill wharves and broad faced structures such as warehouses will likely need to withstand higher magnitude lateral loads, but not uplift. Storage tanks present additional complications due to the potential for punctures and resulting leaks of hazardous or flammable substances. Other objects such as cargo containers and vessels present in ports may create additional hazards if not moored properly by acting as tsunami driven debris which may collide with critical infrastructure. Finally, steel and other metals may corrode should drainage be inadequate wherein the tsunami may leave pools of seawater behind.

The variety of infrastructure types coupled with the number of potential sources of tsunami damage is too extensive to cover comprehensively in one study. Thus the scope of this study is limited to examining the effect of tsunami on open style wharf type structures, which are the most common wharf type in New Zealand. This infrastructure type was chosen as it is one of the most fundamental and critical structural types present in ports, and has an immediate impact on the functionality of these facilities. Previous studies at the University of Auckland have investigated load magnitudes resulting from debris impact and tsunami induced scour (Shafiei, 2015, Shafiei, 2016). Both of these phenomena are difficult to

implement into a structural analysis model for various reasons. Thus, this study aims to characterise the damage to open-type wharf structures resulting from tsunami hydrodynamic loads. The aims of the research presented herein can be summarised as follows:

1. **Research Aim 1: Physical modelling of tsunami loading of wharf structures**
    i. Experimental testing of tsunami uplift from tsunami bore
    ii. Experimental testing of tsunami uplift from solitary wave
    iii. Comparison of uplift loads generated from bore and wave
    iv. Tsunami load characteristics based on design standard estimates
    v. Comparison of tsunami uplift from experimental studies and design standards
    vi. Development of tsunami loading time series for use in structural modelling
2. **Research Aim 2: Computational modelling of wharf damage states from tsunami loads**
    i. Determine characteristics of existing wharf infrastructure in New Zealand
    ii. Generate representative structural models in OpenSees
    iii. Apply tsunami loading time series to structural models over range of wave heights
    iv. Define wharf damage states based on stresses

The structural analysis portion of this research is a first attempt at a ground-up approach and there is little available literature and few related previous studies. Furthermore, a lack of real world data regarding tsunami loads on any infrastructure type is apparent and it is therefore difficult to verify the quantified loads against a realistic scenario. To ensure the most representative possible estimates, two methods were compared for the quantification of tsunami loads: current international design standard loads (based on experimental and computation studies) and University of Auckland experimental results from a wave flume study.

Chapter 2: Quantification of Tsunami Loading

The first step in analysing tsunami damage to port infrastructure is to quantify tsunami loads. Load quantification is an issue which has received much attention in recent years, particularly following the catastrophic Indian Ocean Tsunami of 2004 and Tohoku Tsunami of 2011. Tsunami loading is often broken down into components for the ease of understanding how those loads interact with structures. Most design standards and experimental studies have attempted to quantify lateral components of tsunami hydrodynamic loading. However, certain elevated structure such as wharves and bridges are also subject to uplift loads from rapidly rising water. A review of existing literature reveals only one publication explicitly mentioning and attempting to quantify uplift loads (FEMA, 2008).

2.1 Experimental Loads

Further research is needed to develop reliable estimates for tsunami hydrodynamic uplift loads. Therefore, a significant component of this research was a comprehensive series of experiments carried out in the fluid mechanics laboratory at the University of Auckland which sought to quantify tsunami uplift on scale model wharf structures. This research was carried out in two phases. The first examined loads exerted by a tsunami bore while the second investigated the same loads from an unbroken sinusoidal wave. The purpose of the second study was to determine whether it would be accurate to model tsunami uplift as a solitary wave, simplifying the prediction of the loading characteristics. This research resulted in two conference papers which are presented in the following section (Chen et al., 2015, Popovich et al., 2015).

2.1.1 Publications on Tsunami Uplift Loads

The following pages present the publications listed above.

Quantifying Uplift Loads on Pile Supported Wharf Structures, Part 1: Tsunami Bore

Cheng Chen[1], Bruce W. Melville[1], Seyedreza Shafiei[1], Benjamin G. Popovich[1], Asaad Y. Shamseldin[1], and Liam Wotherspoon[1]
[1] University of Auckland, Auckland, New Zealand; cche841@aucklanduni.ac.nz

Abstract
Tsunamis are shallow water waves which have caused a high toll of casualties, massive economic devastation, and damaged coastal buildings, bridges, highways and harbour facilities. An experimental study of the effects of tsunami bores acting on a wharf-deck structure is presented. The experiments were conducted in a tsunami wave flume (14 metres long by 1.2 metres wide by 0.8 metres high), which features a dry bed condition in front of the deck model. A tsunami bore was generated from an adjacent reservoir by suddenly lifting a sluice gate. The deck model was built on an adjustable sloping shore with heights of 20 cm and 25 cm above the dry bed. Using wave gauges and a video camera, detailed measurements of bore heights and bore velocities were recorded; different cases were used in the experiments, representing different bore strengths. The spatial distributions of the time histories of pressures were captured by pressure sensors. Results show that the time-history of the pressures has three stages: impulsive stage, run-up stage, and quasi-steady stage. The impulsive pressure was measured for different bore strengths, different slamming positions, different slope angles and different ratios of the bore height to the deck height. Some results from the experiments presented in this paper (obtained for a tsunami bore) are compared with those presented in the companion paper (obtained for a solitary wave).

Keywords: Tsunami, Wharves, Ports, Uplift Loads, Bore

1. Introduction

Tsunamis are considered to be shallow water waves [1] and have caused disasters in many areas [2]. In recent years, some catastrophic tsunamis have occurred, such as the 2004 Indian Ocean tsunami [3], the 2010 Chile tsunami [4] and the 2011 Japan tsunami [5].

Previous investigations of tsunami forces acting on both vertical-standing and horizontal-standing structures have been published. Robertson et al. [6] conducted experiments focusing on the fluid forces of a bore impacting a wall/floor system. Measurements of the horizontal and vertical components of the fluid force and pressure acting on a girder bridge due to solitary waves were presented by Araki et al. [7]. Kosa et al. [8] conducted experiments to evaluate tsunami wave forces acting on bridges, while Araki and Deguchi [9] investigated the applicability of the existing prediction methods to estimating the wave force acting on a horizontal plate above a still water level. Robertson et al. [10] carried out a series of experiments in a large wave flume to quantify tsunami bore forces on vertical walls. Rahman et al. [11] revealed the damage mechanism in a bridge girder by assessing the exerted tsunami forces. Al-Faesly et al. [2] investigated the time-history of pressure on a structure for dry- and wet-bed conditions in a flume, and found that the sudden rise of the pressure profile for a wet-bed condition was smaller than that obtained under a dry-bed condition.

However, tsunami bore actions on a pile-supported wharf structure is unclear. So the objective of this paper is focused on modelling a pile-supported wharf-deck structure acted on by a simulated tsunami bore. A companion paper includes results from a parallel study, wherein a similar wharf-deck structure was subjected to loads induced by a solitary wave.

2. Experimental Set-up

The experiments were conducted in the Fluid Mechanics Laboratory at the University of Auckland.

2.1 Tsunami wave flume

The tsunami wave flume is shown in Figure 1. The flume is 14 m long, 1.2 m wide and 0.8 m high. The reservoir is 11 m long, 7 m wide and 0.6 m high, and has a capacity of about 40 m^3 water. The flume and the reservoir are connected by a sluice gate, which is used to suddenly release the water from the reservoir into the flume. The flume can be rapidly drained after each experiment using a drain channel.

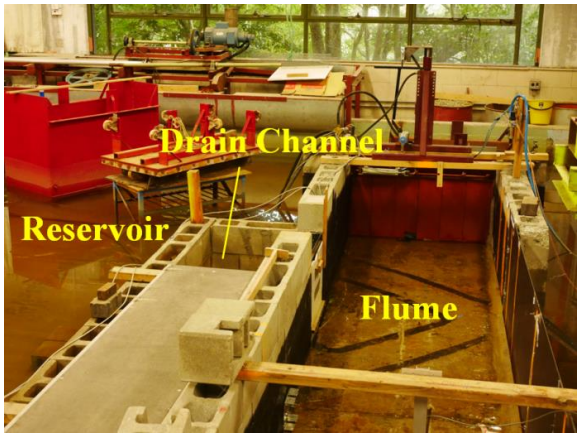

Figure 1 Tsunami wave flume and reservoir

2.2 Sluice gate

The sluice gate consists of a vertically-sliding gate and a shutter gate (Figure 2). The gate opening height and the gate opening time are controlled by a computer. The gate is 1.2 m wide and 0.6 m high. To release the water from the reservoir and generate a tsunami bore, the sliding gate is rapidly raised; the shutter gate opens simultaneously. Different tsunami bore strengths are generated by adjusting the combinations of gate opening heights and reservoir water levels.

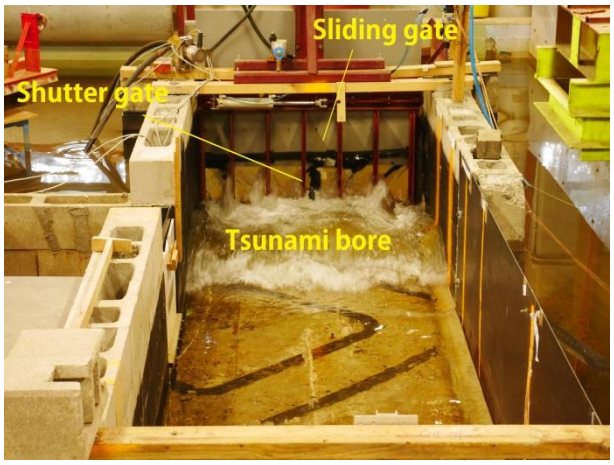

Figure 2 The opening of the sluice gate beginning to generate the tsunami bore.

2.3 Wharf model

A deck-slope-pile model structure was used to simulate a typical wharf (Figure 3). The wharf-deck model was mounted on an adjustable slope allowing modelling of typical beneath-wharf slopes from 20 to 50 degrees. The model deck and slope are plexiglass, and the piles are steel. The horizontal deck is 1.2 m long, i.e. it spans the full width of the flume, and 22 cm wide in the stream-wise direction. The height of the deck is adjustable, from 20 cm to 25 cm above the dry bed.

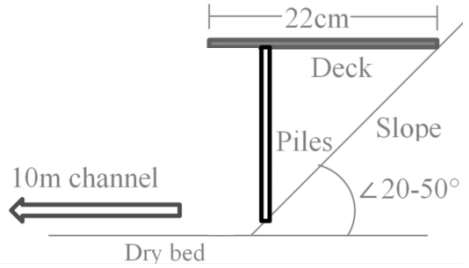

Figure 3 The sketch of the deck-slope-pile structure.

2.4 Wave gauge

A pair of calibrated wave gauges was installed in the flume to measure the bore height in front of the wharf model. The spacing between the two gauges was 1.5 m, allowing the bore velocity to be measured using the time interval required for the tsunami bore to travel between the two wave gauges. A photo of the wave gauges is shown in Figure 4.

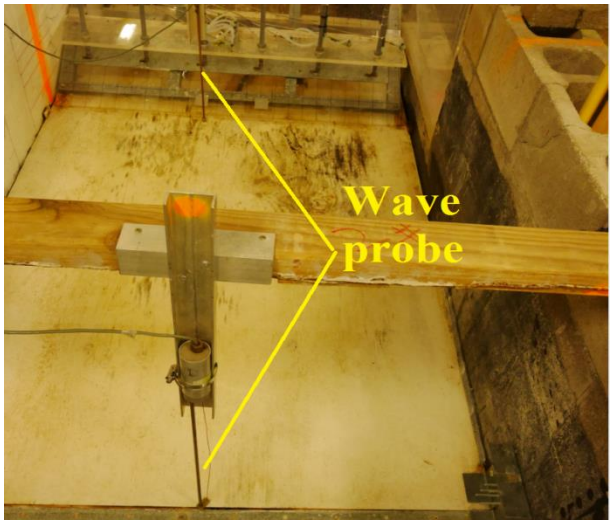

Figure 4 A pair of wave gauges in front of the deck-slope-pile structure.

2.5 Pressure sensor

Five pressure sensors were calibrated and made waterproof using a silicon substance. The pressure sensors were attached to the deck to capture the time-history of uplift pressure loading on the soffit of the deck. Since the wave flume was assumed to be quasi-two dimensional, all five pressure sensors were evenly distributed along the stream-wise centreline (Fig.5) so that any side effect of the flume was reduced as much as possible.

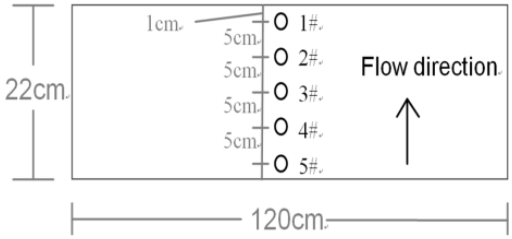

Figure 5 Positions of the pressure sensors on the deck.

2.6 Tsunami wave types

For the tsunami bore experiments presented herein, the range of the ratio of bore height to deck height varies from 0.68 to 1.4, as shown in Table 1. For the parallel study presented in the companion paper (using a solitary wave condition), the equivalent parameter is the ratio of wave height to deck height above the still water level. A comparison of results from this paper and the companion paper is included in the companion paper (Popovich et al. [12]).

Table 1 The ratio of the bore height to the deck height for the tsunami bore experiments.

Tsunami Bore		
Bore Height, h (cm)	**Deck Height, h_d (cm)**	**Ratio**
17	20	0.85
21	20	1.05
22	20	1.10
24.5	20	1.23
28	20	1.40
17	25	0.68
21	25	0.84
22	25	0.88
24.5	25	0.98
28	25	1.12

(Note : For tsunami bore experiment, ratio is bore height to deck height above the dry bed)

3. Results and Discussion

3.1 Bore height and velocity

The velocity of the tsunami front breaking in a coastal zone can be written as follows:

$$u = k\sqrt{gh} \qquad (1)$$

where h is the inundation depth and k is a coefficient representing the front Froude number (Fr).

In this experiment, the bore height and velocity for the tsunami bore travelling in the dry bed flume are shown in Table 2. The Froude number varies from 1.56 to 1.59 due to different bore heights and velocities.

Assuming a representative value of k =1.58, Equation 1 can be written

$$u = 1.58\sqrt{gh} \qquad (2)$$

where h is the bore height in the dry bed flume (in m) and u is the bore velocity (in m/s)

Table 2 Bore height and velocity in the flume

Bore height, h (m)	Bore velocity, u (m/s)	Froude number
0.17	2.04	1.58
0.21	2.24	1.56
0.22	2.34	1.59
0.245	2.46	1.59
0.28	2.61	1.57

3.2 Time history of pressure for different bore strengths

Five different tsunami bore strengths were generated, with heights varying from 0.17 m to 0.28 m. Figure 6 illustrates the time-histories of uplift pressures at the mid-point of the deck (pressure sensor 3#) for a deck height of 25 cm and a slope of 25 degrees. The data were smoothed using a 0.05 s moving mean. The initial time is about 1 second before the tsunami bore strikes the deck. Three different pressures are evident in the plots [13], namely the impulsive pressure, the run-up pressure and the quasi-static pressure. The impulsive pressure is characterized by a significant with a rapid decline. The impulsive pressure is followed by the run-up stage, during which the pressures gradually increased. The run-up stage represents the period immediately after the impulsive stage, during which the tsunami is diverted up the slope. During the quasi-steady stage, the pressure stop increasing, become relatively steady, and then begin to decrease. Eventually, the tsunami bore in the flume receded and the pressure dropped to zero again. As expected, the uplift pressure increased as the bore strength increased. The maximum impulsive pressure for 25 cm deck height and 25 degrees slope was around 10.3 kPa and occurred at the maximum bore strength (0.28 m bore height and 2.61 m/s bore velocity).

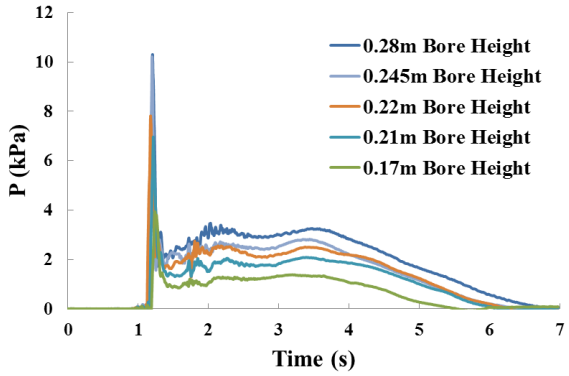

Figure 6 Time-history of pressure for different bore heights (the deck height was 25 cm above the dry bed and the angle of the slope was 25 degree).

3.3 Pressure distribution along centreline in stream-wise direction

The time-histories of the uplift pressures along the stream-wise centreline of the deck is shown in Figure 7, for the bore height of 0.28 m, deck height of 20 cm and slope angle of 25°. The time-histories of pressure distributions are similar for all sensors, with the maximum impulsive pressure reducing gradually from the deck-slope connection to the front edge of the deck. After the initial impact of the bore, pressures at the different positions on the centreline exhibited almost the same magnitudes

i.e. the run-up pressure and quasi-steady pressure are relatively invariant in the stream-wise direction.

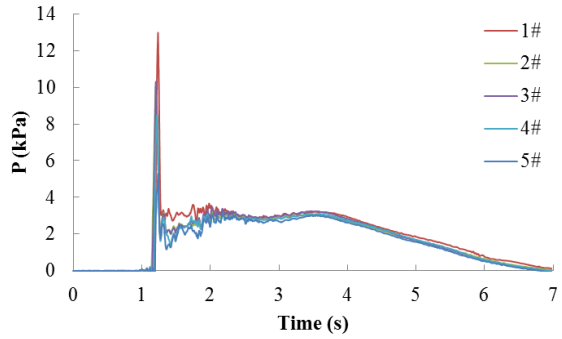

Figure 7 Distribution of the time-histories of pressures in the stream-wise direction. (the slope angle is 25 degree, the deck height is 20 cm, and bore height is 0.28 m)

3.4 Impulsive pressure for different slope angles

The effect of the slope angle on the impulsive pressure (P_i) was investigated by varying the angle of the slope (θ) from 20° to 50°. For these tests, the deck height remained constant at 20 cm (Figure 8) and 25 cm (Figure 9) above the bed, respectively. The plots show that P_i increases with increasing h, as mentioned in section 3.2. However, for most cases, P_i tends to decrease with increasing θ. For example, for h_d = 20 cm and h = 0.28m, P_i is about 11 kPa on the 20° slope, and about 7k Pa on the 50° slope. A comparison of Figure 8 and Figure 9 shows that higher deck height result in lower impulsive pressure, as expected.

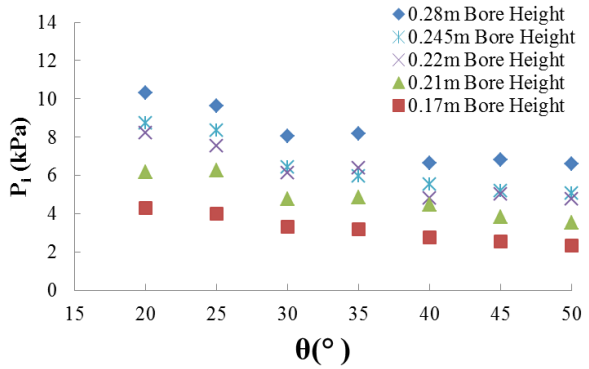

Figure 8 Angle effect on impulsive pressure (the deck height is 20 cm above the dry bed).

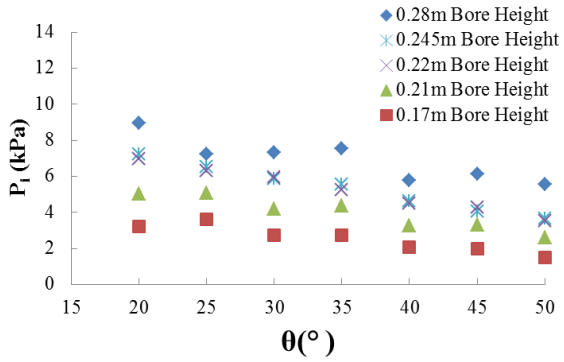

Figure 9 Angle effect on impulsive pressure (the deck height is 25 cm above the dry bed).

3.5 Impulsive pressure for different wave conditions

The relationship between normalized height (h/h_d) and P_i is shown in Figure 10, Figure11 and Figure 12, for 25°, 30° and 35° slopes, respectively. The results indicate that P_i increases with normalized height. For example, for 25 degree slope, P_i increases from 3.6 kPa to 9.6 kPa when (h/h_d) increases from 0.68 to 1.4.

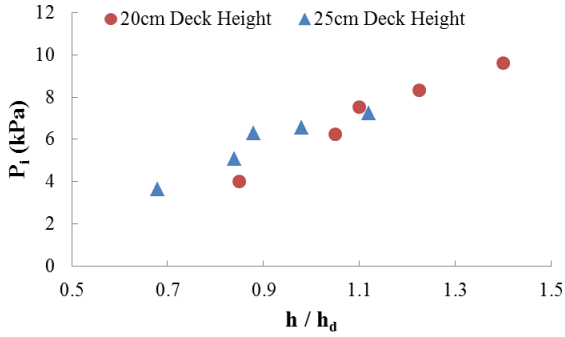

Figure 10 Impulsive pressure for different normalized heights (slope angle is 25 degree).

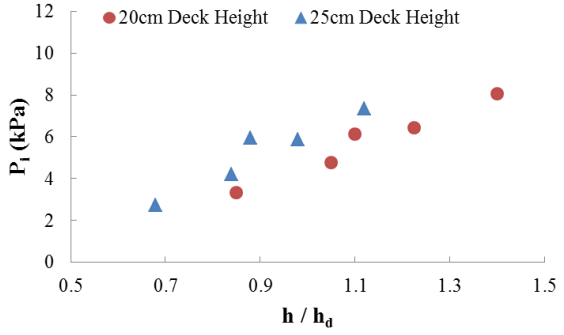

Figure 11 Impulsive pressure for different normalized heights (slope angle is 30 degree).

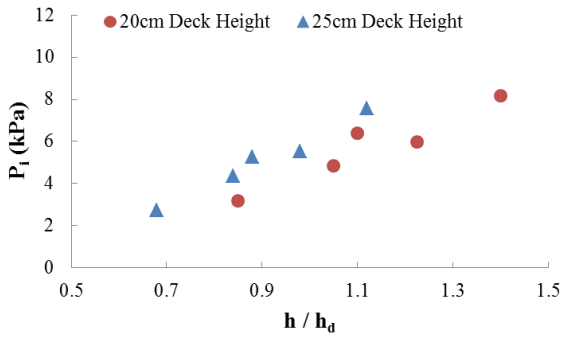

Figure 12 Impulsive pressure for different normalized heights (slope angle is 35 degree).

In Figure 13, normalised pressure (P_n) is plotted against the normalized height. The normalised pressure is the ratio of impulsive pressure to hydrostatic pressure based on bore height, h.

The range of the normalized pressure plotted in Figure 13 ranges from 1.6 to 3.5, showing that the impulsive pressure is much higher than the hydrostatic pressure. Also, the normalised pressure increases as normalised height increases, indicating that either a higher bore or a lower deck produces a higher impulsive pressure.

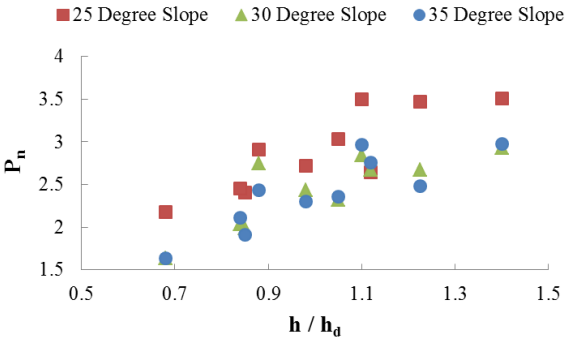

Figure 13 The relationship between Pn and (h/hd).

4. Summary and Conclusion

The following conclusions are drawn from this paper:

- The Froude number in this experiment is around 1.58, which is consistent with typical tsunami bore conditions;
- The time-histories of pressures exhibit an impulsive pressure, a run-up pressure and a quasi-static pressure;
- The uplift impulsive pressure on the soffit of the deck increases with increasing bore strength;
- The impulsive pressure reduced gradually on the stream-wise centreline from the deck-slope connection to the front edge of the deck;
- The impulsive pressure decreases with increasing slope angle;
- Either a stronger bore or a lower deck produces a higher impulsive pressure.

5. References

[1] Thusyanthan, N.I. and Madabhushi, S.G. (2008). Tsunami wave loading on coastal houses: a model approach. Proceedings of the ICE-Civil Engineering. Thomas Telford. Vol. 161, No.2, pp. 77-86.

[2] Al-Faesly, T., Nistor, I., Palermo, D., Cornett, A. (2011). Simulated tsunami bore impact on an onshore structure. 20th Canadian Hydrotechnical Conference. pp. 14-17.

[3] Hirata, K., Satake, K., Tanioka, Y., Kuragano, T., Hasegawa, Y., Hayashi, Y., Hamada, N. (2006). The 2004 Indian Ocean tsunami: Tsunami source model from satellite altimetry. Earth, planets and space. Vol. 58, No. 2, pp. 195-201.

[4] Fritz, H.M., Petroff, C. M., Catalan, P. A., Cienfuegos, R., Winckler, P., Kalligeris, N., Weiss, R., Barrientos, S.E., Meneses, G., Valderas-Bermejo, C., Ebeling, C., Papadopoulos, A., Contreras, M., Almar, R., Dominguez, J.C., Synolakis, C.E. (2011). Field survey of the 27 February 2010 Chile tsunami. Pure and Applied Geophysics, Vol. 168, No. 11, pp. 1989-2010.

[5] Fritz, H.M., Phillips, D.A., Okayasu, A., Shimozono, T., Liu H., Mohammed, F., Skanavis, V., Synolakis, C., Takahashi, T. (2012). The 2011 Japan tsunami current velocity measurements from survivor videos at Kesennuma Bay using LiDAR. Geophysical Research Letters, Vol. 39, No. 7. (http://dx.doi.org/10.1029/2011GL050686)

[6] Robertson, I., H. Riggs, and Mohamed, A. (2008). Experimental results of tsunami bore forces on structures. ASME 2008 27th International Conference on Offshore Mechanics and Arctic Engineering. American Society of Mechanical Engineers. pp. 509-517.

[7] Araki, S., Ishino, K., Deguchi, I. Stability of girder bridge against tsunami fluid force. (2011). Coastal Engineering Proceedings. Vol. 1, No. 32, pp. structures. 56.(https://journals.tdl.org/icce/article/download/1413/pdf_126)

[8] Kosa, K., Miyahara, K., Shoji, M. (2010). Experimental study for estimating tsunami forces acting on bridge girders. Proceeding of 26th US–Japan Bridge Engineering Workshop. Public Works Research Institute Tsukuba, Japan. pp. 1-14.

[9] Araki, S. and Deguchi, I. (2012). Prediction of wave force acting on horizontal plate. Coastal Engineering Proceddings. Vol. 1, No. 33, pp. structures. 52 (http://dx.doi.org/10.9753/icce.v33.structures.52).

[10] Robertson, I., Paczkowski, K., Riggs, H.R., Mohamed, A. (2013). Experimental investigation of tsunami bore forces on vertical walls. Journal of Offshore Mechanics and Arctic Engineering. Vol. 135, No. 2, pp. 021601-(1-8).

[11] Rahman, S., Akib, S., Shirazi, S. (2014). Experimental investigation on the stability of bride girder against tsunami forces. Science China Technological Sciences, Vol. 57, No. 10, pp. 2028-2036.

[12] Popovich, B.G., Wotherspoon, L., Shafiei, S., Chen, C., Melville, B.W., Shamseldin, A.Y. (2015). Quantifying Uplift Loads on Pile Supported Wharf Structures, Part 2: Solitary Wave. Paper presented at the Australasian Coasts & Ports Conference 2015, Auckland, New Zealand.

[13] Al-Faesly, T., Palermo, D., Nistor, I., Cornett, A. (2012). Experimental modelling of extreme hydrodynamic forces on structural models. International Journal of Protective structures, Vol. 3, No. 4, pp. 477-505.

Quantifying Uplift Loads on Pile Supported Wharf Structures, Part 2: Solitary Wave

Benjamin G. Popovich[1], Liam Wotherspoon[1], Seyedreza Shafiei[1], Cheng Chen[1], Bruce W. Melville[1], and Asaad Y. Shamseldin[1]

[1] Department of Civil Engineering, University of Auckland, Auckland, New Zealand;
b.popovich@countermail.com

Abstract

This study attempts to quantify uplift loads from a solitary wave and assess the applicability of those findings to tsunami loading. A representative wharf model at a 1/90 scale was constructed and attached to an adjustable slope which was varied from 25° to 35° to study the effects of the coastal bathymetry on which the structures sit, and peak uplift pressures were recorded over a range of wave amplitudes. A series of probability distributions were created that detailed the likelihood that the pressure from a given wave amplitude would not exceed a certain value. Typical uplift pressures at the 50th percentile ranged from approximately 2000 to 7000 Pa. This variation was dependant on wave amplitude, but not slope angle which appeared to have little effect. This study was performed in conjunction with another which quantified uplift pressures for an identical structure from a tsunami bore. The peak uplift magnitudes from a solitary wave were found to be approximately one-third the magnitude for a tsunami bore.

Keywords: Tsunami, Wharves, Ports, Uplift Loads, Solitary Wave

1. Introduction

Engineers have long known that tsunami have the potential to generate catastrophic loads on infrastructure, particularly infrastructure located near coastlines. Although this idea is made obvious by the remnants of recent devastating tsunami, quantification of those loads and development of design standards intended to mitigate their impact remains a difficult task. Most publications and early standards separate the forces into components and recommend load combinations for various scenarios and structural components [2,4,5]. Numerous studies have attempted to quantify the horizontal loads from tsunami while few have considered the vertical hydrodynamic, or uplift, loads exerted on raised structures [5,6]. Field investigations following the 2004 Indian Ocean Tsunami and 2011 Tohoku Tsunami revealed port infrastructure that had been damaged or destroyed due to uplift loads from the tsunami [1,7]. This paper presents the initial results from an experimental study that aims to quantify the wave uplift forces on pile supported wharf structures. In this study, the waves were solitary waves with the point of interest being the peak impact uplift pressure exerted on the structure. This research was performed in parallel with another study investigating the pressure distribution on an identical scaled structure from a model tsunami bore [3]. This comparison gives an indication as to whether these solitary waves are sufficient to represent the peak impact uplift pressures from a tsunami bore.

2. Methodology

2.1 Overview and Experimental Parameters

The laboratory testing presented in this paper utilised a wave flume with dimensions 25 metres long, 81 cm wide, and 110 cm deep, a scaled wharf structure, and an artificial slope on which the structure rested. The ultimate goal was to quantify the peak uplift loads on the structure based on a number of predetermined variables. The potential variables associated with the wharf structure included the length, width, and thickness of the deck, and the slope on which the structure was founded. Variables associated with the wave characteristics included amplitude, celerity, and the initial depth of water. Due to the large number of potential variables, it was necessary to limit the overall scope to include only a few variable parameters while holding the remainder constant. Here the parameters we focus on are the slope angle on which the structure lies and the amplitude of the impacting wave.

2.2 Wharf and Artificial Slope Model

The dimensions of the wharf model were representative of typical existing New Zealand wharf structures. Additionally, the height of the deck relative to the still water level was also representative of New Zealand conditions. The scale of the model was determined by comparing the maximum expected tsunami amplitude in New Zealand and the maximum wave amplitude generated by the wave paddle. The ratio of these parameters resulted in a scale of 1/90.

The wharf model consisted of an acrylic deck measuring 22.2 cm wide by 81 cm long by 2.2 cm thick. As flexibility was a factor that may have impacted the pressure recordings, acrylic was chosen for its relative stiffness. The deck was supported by a back end hinge which was fixed to the slope. Two threaded rods acting as piles supported the front end, further restricting the flexibility of the wharf structure.

An artificial slope was placed in the flume to model the slope on which a typical wharf structure would

rest. Figures 1 and 2 show schematics of the deck and slope model used in this experimentation in plan and profile views respectively.

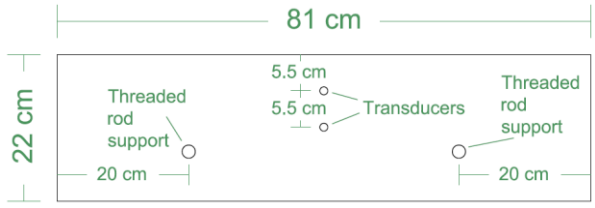

Figure 1: Schematic of wharf deck model detailing dimensions.

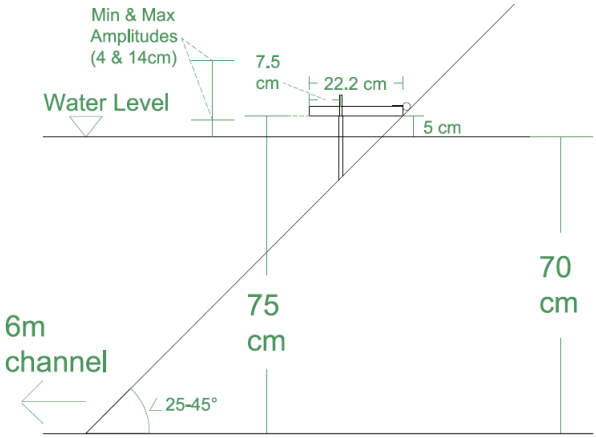

Figure 2: Schematic of wharf model and artificial slope detailing dimensions used.

The slope was constructed six metres from the wave paddle, as the energy loss and corresponding wave amplitude reduction associated with the entire 25 metre concrete channel proved too great. The angle of the slope was varied throughout testing. In many scenarios, wharves lie next to dredged seabeds, but the bathymetry directly underneath the wharf is sloped. The coastal slopes typically range from 20° to 45°. This study investigated impacts at angles of 25°, 30°, and 35°. As the slope angle changed, coupled variations were required in the length of the slope in order to maintain the deck height.

2.3 Data Instrumentation

The wave flume was equipped with three wave probes, two of which were placed one and six metres respectively from the wave paddle. These recorded wave heights immediately after generation and directly in front of the slope. The location of the third wave probe was varied with the angle of the slope, and was always placed immediately before the wharf model in order to record wave heights upon impact. These wave probes were also used to calculate wave celerity by isolating the time steps of peak amplitude readings.

Two differential pressure transducers were attached to the centreline of the deck. These recorded impact pressure through a small hole in the deck as the wave struck. One transducer was placed 5.5 cm from the rear of the wharf while the other was placed at the centre of the wharf deck. This paper will refer to each as “rear transducer” and “centre transducer” respectively. The width of the channel required that pressure transducers be concentrated in the centre of the structure in order to eliminate data contamination from wave reflection. The transducer sampling rate was set to 100 Hz, which was adequate for capturing low period peak pressures. Figure 3 shows the wharf model, slope, and wave probes used in this experimentation.

Figure 3: Photo of wharf model, artificial slope, and wave probes. Note that the water level in the picture was not the water level used in experimentation.

2.4 Wave Characteristics

Waves were generated by a wave paddle controlled by a Wavetek Model 75 Arbitrary Waveform Generator, which was capable of varying the wave period and amplitude. The wave controller allowed the user to vary settings that controlled the degree of motion of the wave paddle, resulting in different generated wave amplitudes. Initial tests were conducted without the structure present in order to determine the wave amplitudes the paddle was capable of generating. Typical wave amplitudes ranged between 4 and 14 cm.

Celerity and wave amplitude could not be varied independently. According to small amplitude wave theory, the waves generated mostly fell within the category of shallow-water waves. The theoretical celerity of a shallow water wave (C) varies only with water depth (d) as seen in Equation 1. The third variable, g, is the acceleration of gravity.

$$C = \sqrt{gd} \qquad (1)$$

Small amplitude wave theory relies on several simplifying assumptions and generally applies to theoretical oceanic gravity waves. Therefore, the calculated celerity was expected to vary slightly from the theoretical value. Figure 4 shows the

horizontal celerities for 280 runs over various wave heights. These celerities were calculated for respective runs by examining the wave amplitude time series recorded by the first two wave probes and the distance between these probes. .

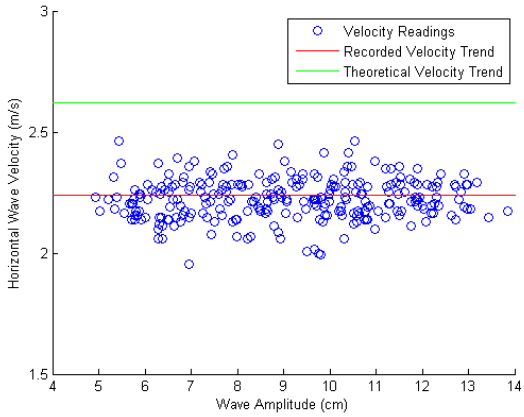

Figure 4: Horizontal wave celerity for 280 runs. The red line indicates the mean of the recorded velocities and the green indicates the theoretical celerity according to Small Amplitude Wave Theory.

The mean measured horizontal celerity was slightly lower than the theoretical value. As expected, the celerity did not vary with wave height. As the water depth was held constant, the wave amplitude was used as the parameter by which the pressure peaks were compared rather than velocity.

At each slope angle, eight separate wave controller settings were tested in order to confidently determine the range of pressures from the respective wave amplitudes. Wave amplitudes referenced in this paper refer to the generated values recorded by the first probe, closest to the wave paddle. 35 waves were generated at each setting, resulting in a total of 840 runs.

2.5 Interpretation of Experimental Data

As the research interest is the instantaneous uplift load created by the rising water, the parameters used in the interpretation of the data were the peak wave height and the first peak pressure reading in the transducers. It was impossible to eliminate any successive trace waves and create a truly solitary wave, and therefore subsequent pressure peaks were evident following the initial reading in most cases. These peaks were ignored as the point of interest was the load resulting from the leading wave crest. Figures 5 and 6 present representative data readings by a wave probe and transducer respectively and highlight the region of data that was isolated and utilised.

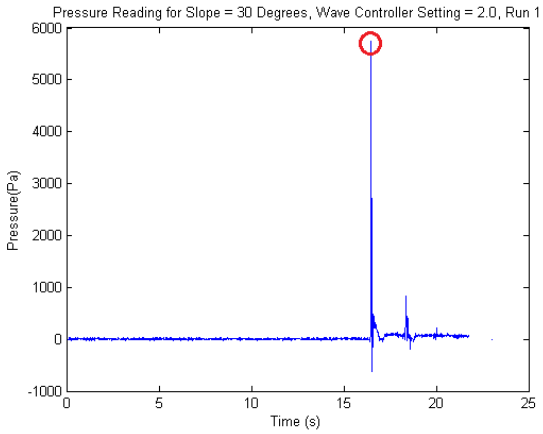

Figure 5: Sample pressure reading as recorded by differential pressure transducer.

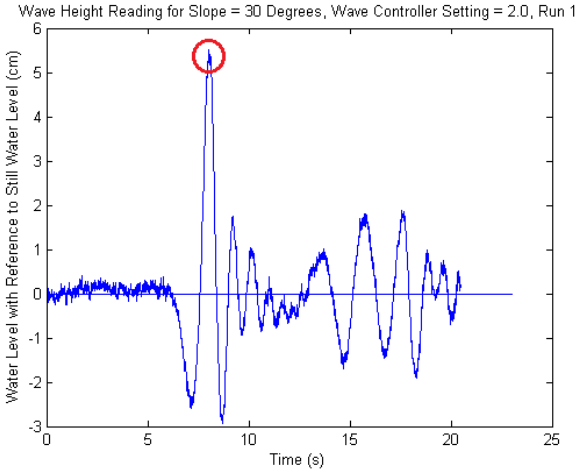

Figure 6: Sample water level reading as recoded by wave probe.

3. Experimental Results

During testing, certain factors were noted that may have impacted the results. First, at no point over any of the three slopes did the solitary waves break from instability. Therefore, all impact was the result of unbroken wave uplift. At higher angles, a runup effect was noted. This resulted in the wave amplitudes being slightly higher greater upon impact. In every case, the wave appeared to strike the deck uniformly with little turbulence. In cases where the wave amplitudes were greater than the wharf height, the wave broke over the wharf. While there was an indefinitive direct trend between wave amplitude and peak pressure, the best fits were negative quadratic functions, suggesting the increase in pressure coinciding with increasing amplitudes mitigated at greater wave heights. One possible explanation was the breaking of the wave over the structure.

3.1 Wave Amplitudes

A range of wave controller settings were used to generate the wave amplitudes summarised in Figure 7. The mean and standard deviation were recorded over 105 runs on each amplitude setting. As there was a significant degree of variation in the

wave amplitude generated by each setting, it was necessary to redistribute the runs in terms of the amplitudes rather than the controller setting. Ultimately, the decision was made to break down wave amplitudes into two centimetre intervals. No significant variation in the corresponding impact pressure was evident within each interval. The recalculated categories and mean amplitudes are presented in Figure 8.

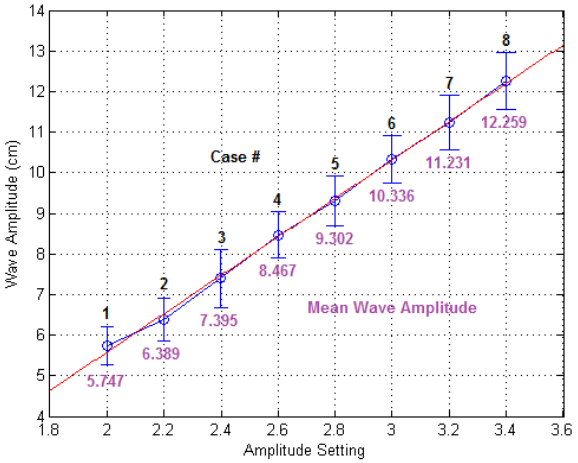

Figure 7: Range of wave heights within each wave controller setting. The red circles indicate the mean values.

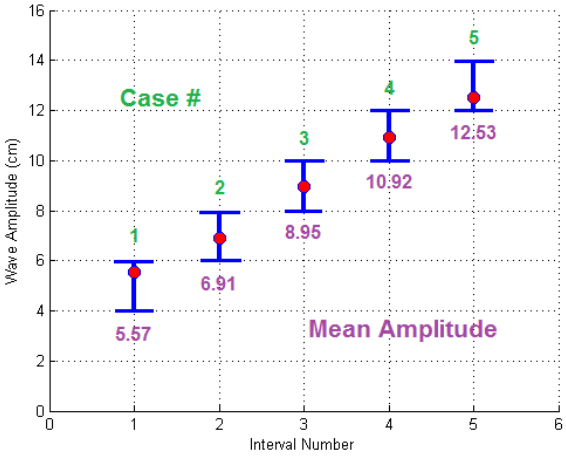

Figure 8: Range of wave heights within each interval used in the data analysis. The red circles indicate the mean values.

3.2 Relationship between Peak Pressure and Amplitude

A large degree of variation in the peak pressure was evident for each wave amplitude, most likely due to the fact that all impacts were from an unbroken wave. Figure 9 shows the peak wave height and peak pressure data for all runs performed on a 35 degree slope clearly indicating this variability in the results. With a coefficient of determination (R^2) of 0.1849, no reliable correlation is evident other than a general, increasing trend. This trend was evident for the other slope angles used in this study.

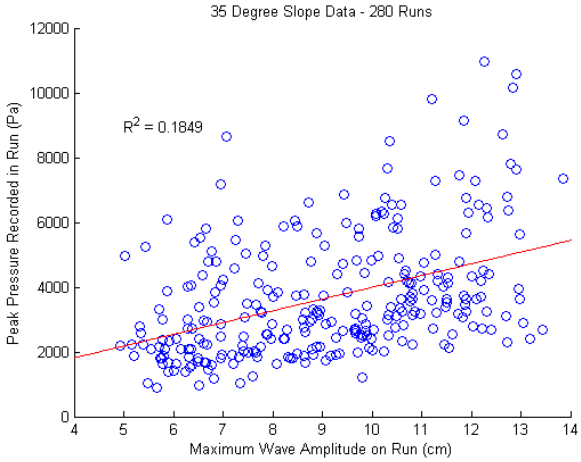

Figure 9: Relationship between peak pressure and wave amplitude for a 35° slope angle. The red line is the simple linear fit for the data.

A more beneficial method of presenting the results is in the context of a probability distribution of peak pressures. This allowed for an examination of the range of pressures which were be exerted from uplift. Using the amplitude categorisation discussed in Section 3.1, most pressure readings were centred about a mean value with a few high outliers slightly skewing the distribution.

These distributions represented the probability that the peak pressure produced by a given wave height will not exceed a certain value. Figure 10a, b, and c respectively show the cumulative probability distributions for 25°, 30°, and 35° respectively in the centre transducer. It should be noted that these are theoretical distributions. However, when compared to the empirically calculated equivalents, the results were nearly identical.

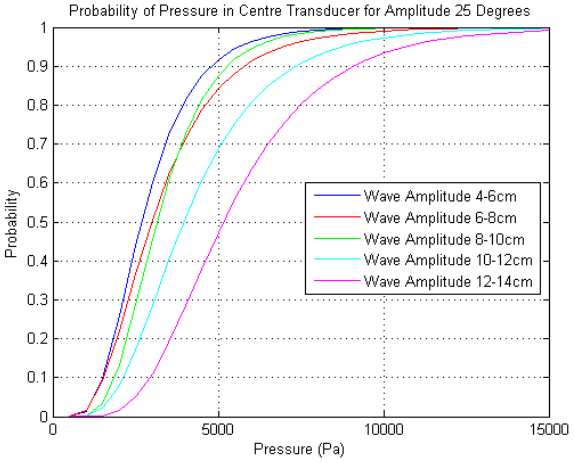

Figure 10a: Cumulative probability distribution functions for all wave amplitudes recorded on a 25° slope.

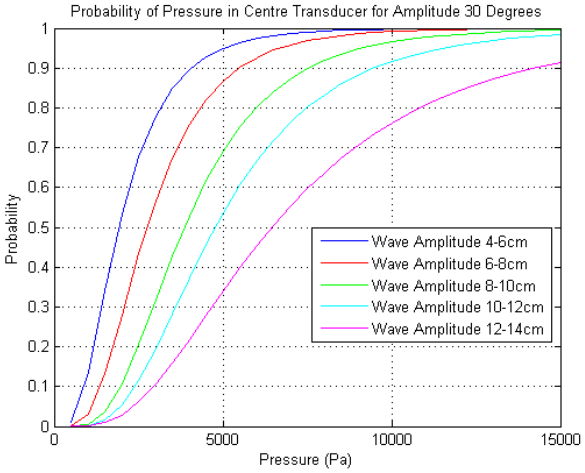

Figure 10b: Cumulative probability distribution functions for all wave amplitudes recorded on a 30° slope.

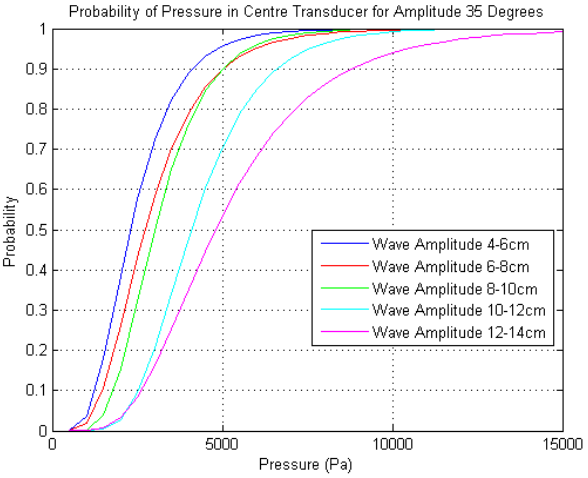

Figure 10c: Cumulative probability distribution functions for all wave amplitudes recorded on a 35° slope.

Similar distributions were developed for the rear transducer. While no consistent trend was apparent between the centre and rear transducers, the pressure peaks were roughly equivalent in most cases. These results suggest that the wave strikes the underside of the deck approximately uniformly if spanning a sufficient wavelength.

3.3 Effect of Slope Angle

In order to evaluate the impact of the slope angle on which the wharf lies, the distributions were contrasted by examining the differences in probability between 25°, 30°, and 35° curves for each case.

In most cases, the 35° distribution consisted of the lowest peaks, suggesting that greater slopes reduce the uplift pressure. However, the lack of a consistent relationship between 25° and 30° draws this possibility into question. In order to conclusively determine whether there is a consistent relationship, more angles must be tested.

The runup effect noted in Section 3 may have contributed to discrepancies in a definable trend. However, the differential magnitude in many of these probability distributions would not be nearly accounted for strictly by accounting for the slight amplitude variation. The possibility that slightly higher waves would break over the deck more often and the perceived effect of that breaking may have also contributed to skewed distributions.

3.4 Comparison with Tsunami Bore Loads

A simultaneous study was carried out at the University of Auckland in which identical load types were recorded for a tsunami bore on an identical structure [3]. While the goal was to compare the impact pressures, the two wave types were shown to result in different types of impacts. Whereas a solitary wave generates an instantaneous pressure spike, a tsunami bore exerts a pressure spike upon initial impact followed by a sustained hydrodynamic force. In spite of the procedural differences between the two studies, comparisons may be drawn between the peak pressure magnitudes achieved upon initial impact.

As the tsunami bore study varied the bore height and the height of the deck above sea level, the ratio of the wave/bore height to the height of the deck is used to compare each study. Two applicable scenarios apply where bore heights of 21 and 28 cm result in approximately equal ratios with solitary wave amplitudes of 5.25 and 7 cm respectively. Peak uplift pressure was typically higher in the case of a tsunami bore. For the lowest bore height, the pressures varied based on the slope, but generally encircles 6000 Pa. For the corresponding solitary wave, the pressures ranged from 2000 to 2500 Pa at the 50th percentile. Even the 90th percentile values, which ranged between 4000 to 5000 Pa, fell below the pressures produced by the bore. Similar comparisons for the all three cases show that the peak pressure ratios (using the 50th percentile values for solitary cases) for identical wave-deck height ratios were approximately one-third.

In general, reducing the slope angle caused the uplift pressure to increase in the case of the tsunami bore. While this relationship is not nearly as clear for a solitary wave, every bore height presents the same trend [3].

4. Conclusions

Using a 1/90 scale model of a wharf on an artificial, adjustable slope, wave uplift was quantified for a solitary wave condition. The range of pressures recorded over various wave heights led to the development of probability distribution functions detailing the likelihood of an impact pressure remaining under a certain value. It is difficult to effectively assign a definitive relationship between wave height and uplift pressure. The angle of the

slope on which the wharf rests has little perceived impact on the magnitude of the pressure. Finally, the peak uplift impact pressure created by a tsunami bore is larger than the same load for a solitary wave. This study found the solitary wave peak uplift pressure to be approximately one-third of the tsunami bore pressure.

5. References

[1] Akiyama, M., Frangopol, D. M., Arai, M., & Koshimura, S. (2012). *Probabilistic Assessment of Structural Performance of Bridges Under Tsunami Hazard*. Paper presented at the Structures Congress 2012.

[2] CCH. (2000). City and Council of Honolulu Building Code. In: Department of Planning and Permitting of Honolulu Hawaii.

[3] Chen, C., Melville, B. W., Shafiei, S., Popovich, B. G., Shamseldin, A. Y., & Wotherspoon, L. (2015). *Quantifying Uplift Loads on Pile Supported Wharf Structures, Part 2: Tsunami Bore*. Australasian Coasts & Ports Conference 2015, Auckland, New Zealand, submitted.

[4] FEMA. (2008). Guidelines for the Design of Structures for Vertical Evacuation from Tsunamis: Federal Emergency Management Agency.

[5] FEMA. (2011). *Coastal Construction Manual* (Fourth ed.): Federal Emergency Management Agency.

[6] Kosa, K., Nii, S., Miyahara, K., & Shoji, M. (2011). Experimental Study for Estimating Tsunami Forces Acting on Bridge Girders. *Proceedings of JSCE*.

[7] Nistor, I., Palermo, D., Cornett, A., & Al-Faesly, T. (2012). *Experimental and Numerical Modeling of Tsunami Loading on Structures*. Paper presented at the International Conference of Coastal Engineering 2012, Santander, Spain.

2.2 Design Standards

Numerous building codes and design standards have attempted to account for tsunami loads in coastal construction. While some explicitly mention and quantify tsunami loads, others represent tsunami through typical wave or flood loads. As new research comes available, these simplifications become obsolete. The three publications which explicitly quantify tsunami loads and which will be considered herein are FEMA's Coastal Construction Manual (FEMA, 2011) and Guidelines for the Design of Vertical Evacuation Structures from Tsunami (FEMA, 2008) and City and County of Honolulu Building Code (CCH, 2000). This section presents each relevant component to tsunami loading and the equations that each design standard provides.

2.2.1 Lateral Hydrodynamic Load

The hydrodynamic force, also known as the drag force, refers to the friction that occurs as water moves around a structure. In most cases, the hydrodynamic force is considered uniform across the width of an entire structure, though due to the turbulent nature of a tsunami, this assumption may prove unreliable. Typically, this force is a function of the flow velocity and a drag coefficient, though a derivation may have subtle, and sometimes significant, differences (Palermo 2008).

The City and County of Honolulu Building Code defines the drag force using Equation 1 (CCH 2000).

$$F_D = \frac{\rho C_D A u^2}{2} \qquad \text{(Eq. 1)}$$

ρ = Density of Water

C_D = Drag Coefficient

A = Area of the Submerged Face Normal to the Direction of Flow

u = Velocity of Flow Relative to Body

The drag coefficient is defined as 1.0 for circular piles, 2.0 for square piles, and 1.5 for wall sections. FEMA provides the same equation in Coastal Construction Manual, but defines the drag coefficient differently. For square or rectangular piles, the value is 2.0, and for round piles, 1.2. For all other shapes, the coefficient is based on the ratio between the width of an object and its height if fully submersed and the water depth if not. The values are summarized in Table 1 (FEMA 2010).

Table 1: Values for drag coefficient, C_D (FEMA 2010)

Width-to-Depth Ratio	**C_D**
1-12	1.25
13-20	1.3
21-32	1.4
33-40	1.5
41-80	1.75
81-120	1.8
>120	2.0

In Guidelines for Structures for Vertical Evacuation from Tsunami, FEMA redefines the hydrodynamic equation to make it more suitable for tsunami loads, rather than typical wave loads. The total force is defined in Equation 2 (FEMA 2008).

$$F_D = \frac{1}{2}\rho C_D B (hu^2)_{max} \quad \text{(Eq. 2)}$$

ρ = Density of Water

C_D = Drag Coefficient

B = Breadth of Structure Normal to Flow Direction

$(hu^2)_{max}$ = Maximum Moment Flux per Unit Mass

FEMA recommends that the drag coefficient be taken as 2.0 in all situations involving tsunami. The combination of flow velocity and depth create the moment flux per unit mass.

It is stressed that the maximum flux must be used. Since the maximum flow velocity and depth are unlikely to occur at the same time, this is defined as $(hu^2)_{max}$ rather than $(h_{max}u^2_{max})$. FEMA (2008) also defines an approximation for this quantity in Equation 3.

$$(hu^2)_{max} = gR^2\left(0.125 - 0.235\frac{z}{R} + 0.11\left(\frac{z}{R}\right)^2\right) \quad \text{(Eq. 3)}$$

g = Acceleration of Gravity

R = Design Runup Elevation (1.3 Time the Maximum Runup Elevation)

Z = Ground Elevation at the Base of the Structure (With Datum at Sea Level)

2.2.2 Wave Slam

Wave Slam refers to the force generated when the leading edge of a surge of water contacts a structure. This is a high magnitude, low duration force. Each standard defines it differently, suggesting that there is a high level of uncertainty related to the quantification of wave slam. In Coastal Construction Manual, FEMA defines wave slam via Equation 4 (FEMA 2011).

$$F_S = \rho g C_S d h w \quad \text{(Eq. 4)}$$

ρ = Density of Water

g = Acceleration of Gravity

C_S = Slam Coefficient = 2.0

d = Stillwater Flood Depth

h = Vertical Distance the Wave Crest Extends Above the Bottom of the Floor Joist

w = Width of Floor Beam or Joist Struck by Wave Crest

The slam coefficient is recommended to be 2.0. In Guidelines for Structures for Vertical Evacuation from Tsunami, FEMA simplifies the equation and merely defines it as 1.5 times the hydrodynamic load, shown in Equation 5 (FEMA 2008).

$$F_S = 1.5 * F_D = 1.5 * \frac{1}{2}\rho C_D B(hu^2)_{max} \quad \text{(Eq. 5)}$$

F_D = Drag Force as Defined by FEMA (2008)

ρ = Density of Water

C_D = Drag Coefficient

B = Breadth of Structure Normal to Flow Direction

$(hu^2)_{max}$ = Maximum Moment Flux per Unit Mass

The City and County of Honolulu Building Code has yet another numerical derivation for this force, shown in Equation 6 (CCH 2000).

$$F_S = 4.5\rho g h^2 w \quad \text{(Eq. 6)}$$

ρ = Density of Water

g = Acceleration of Gravity

h = Surge Height

w = Width of Wall Normal to Flow

2.2.3 Hydrodynamic Uplift

The uplift force is a dynamic force separate from buoyancy which occurs when a tsunami flows underneath an elevated structure causing the water level to rise rapidly and exert a high magnitude load on the base. A notable lack of literature examining uplift loads is apparent when compared to lateral tsunami loads. Of all the standards examined during this study, the only that mentioned and attempted to quantify this load is Guidelines for the Design of Structures for Vertical Evacuation from Tsunami. The recommended value for the uplift force is shown in Equation 7 (FEMA 2008).

$$F_u = \frac{1}{2} C_u \rho A_f {u_v}^2 \quad \text{(Eq. 7)}$$

C_u = Uplift Coefficient = 3.0

ρ = Density of Water

A_f = Area of Floor Panel

u_v = Vertical Velocity of Water

FEMA concedes that this is a rough estimate and can only be used until better research becomes available. Kosa et al. (2011) performed a series of experiments involving lateral and uplift forces on bridge girders which resulted in quantification of these loads. Though the results were different for broken versus unbroken waves, Equation 8 resulted for uplift force which is based on the height of the wave and the position of the girder (Kosa et al. 2011).

$$Q_z = \rho BW\left(0.53a_H - \frac{1}{2.18Z}\right) \quad \text{(Eq. 8)}$$

ρ = Density of Water

B = Length of Face

W = Width of Face

a_H = Wave Height

Z = Height of Girder

It should be noted that both of these equations are derived for the specific application of structure through which the tsunami may flow. This is not the same in the case of a wharf where the back end is fixed to the coast. This may increase the magnitude of the load on the underside of the wharf as a result of air and water entrapment, hence why mitigation techniques typically include perforated or gapped decks through which the tsunami may penetrate.

2.3 Comparison of Experimental and Design Based Uplift Loads

Tsunami uplift loads require more study and experimentation in order to verify the approaches and estimates that are in current use. The experimental testing carried out for this report sought to verify or discredit the design code based approximations through empirical study. Although the experimentation results consisted of more variation in load magnitude as the wave height increased, the trend of increasing loads presented good agreement with uplift loads calculated from FEMA (2008). These results are shown in Figure 1. It should be noted that this comparison does not include the initial impact pressures identified in experimental testing, and instead focuses on the steady state magnitude of this experimental time series (summarised in Section 2.1.1).

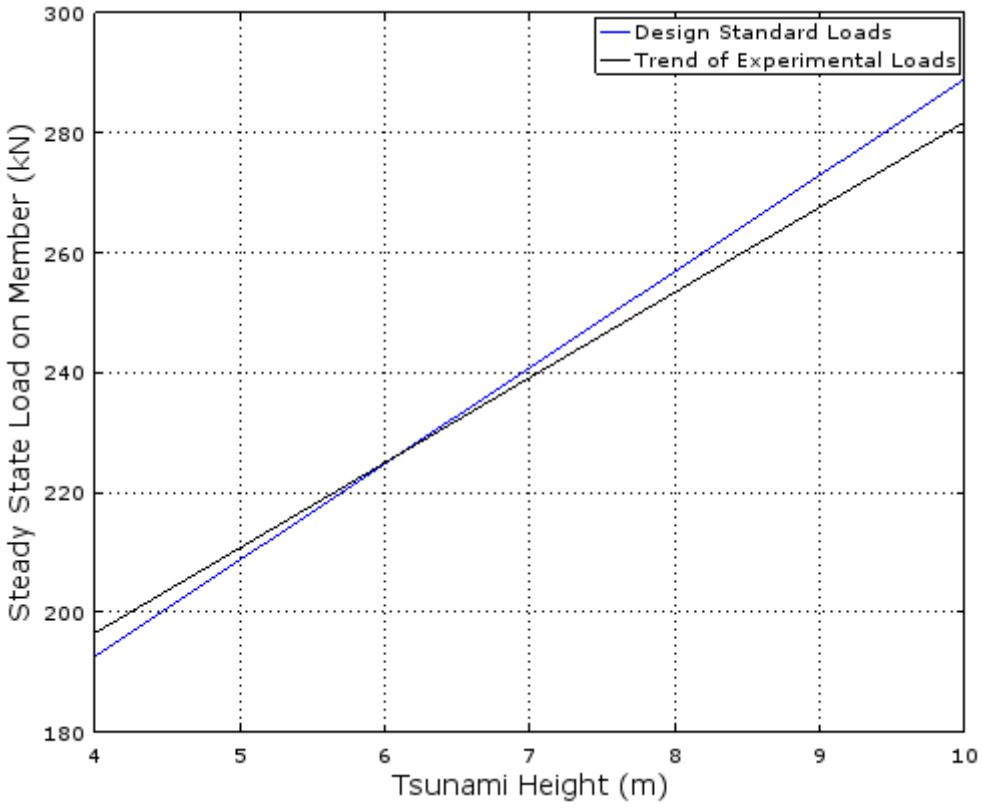

Figure 1: Comparison of tsunami uplift loads as calculated by design standards and from experimental testing.

Chapter 3: Computational Modelling of Impact of Tsunami Uplift Loading on Wharf Structures

The second phase of research involved developing structural wharf models upon which the tsunami loads were applied. The analysis of these models resulted in predictive damage to the structures from tsunami of various wave heights. These structural wharf models were developed in OpenSees (Open System for Earthquake Engineering Simulation), an open-source nonlinear structural analysis framework built on the TCL programming language (Tool Command Language).

The representative models utilized in this study were developed using a range of construction drawings and other documentation from New Zealand port companies. Thus, the models are representative of a number of geometric, material, and geotechnical characteristics of existing wharf infrastructure within New Zealand. There is a larger range of wharf characteristics and types outside the models presented herein. However the aim of this study is not to model all different wharf types.

The base structural model represents an open-style, pile supported wharf. While solid fill and semi-solid fill wharves are present in limited number, the overwhelming majority of New Zealand wharves are open-style. The development methodology and syntax of the computational model allows for easy modification of the structure's characteristics. Thus the base model can be changed to test different materials, sections, elements, and geometric configurations.

A two-dimensional model was used in this analysis, as the form of an open-style wharf repeats itself (in bays) along the shoreline. By assuming propagation of the tsunami bore in line with each bay of the wharf, a single line of piles perpendicular to the shoreline is modelled. A two-dimensional model only allows for examination of stresses and application

of loads horizontally and vertically, but not out of plane. The geometry of each 2-D model consisted of six reinforced concrete piles, each 18 metres long (including below ground sections), topped by a pile cap and a deck. The piles are separated by a distance of two metres, giving the structure a total breadth of ten metres. The piles are embedded into a shore slope at a 45 degree angle, a representative slope for New Zealand shores. Pile bays (the distance between piles parallel to the shore), which were also considered in model development, typically ranges from six to ten metres at New Zealand ports. This model is visually shown in Figure 2.

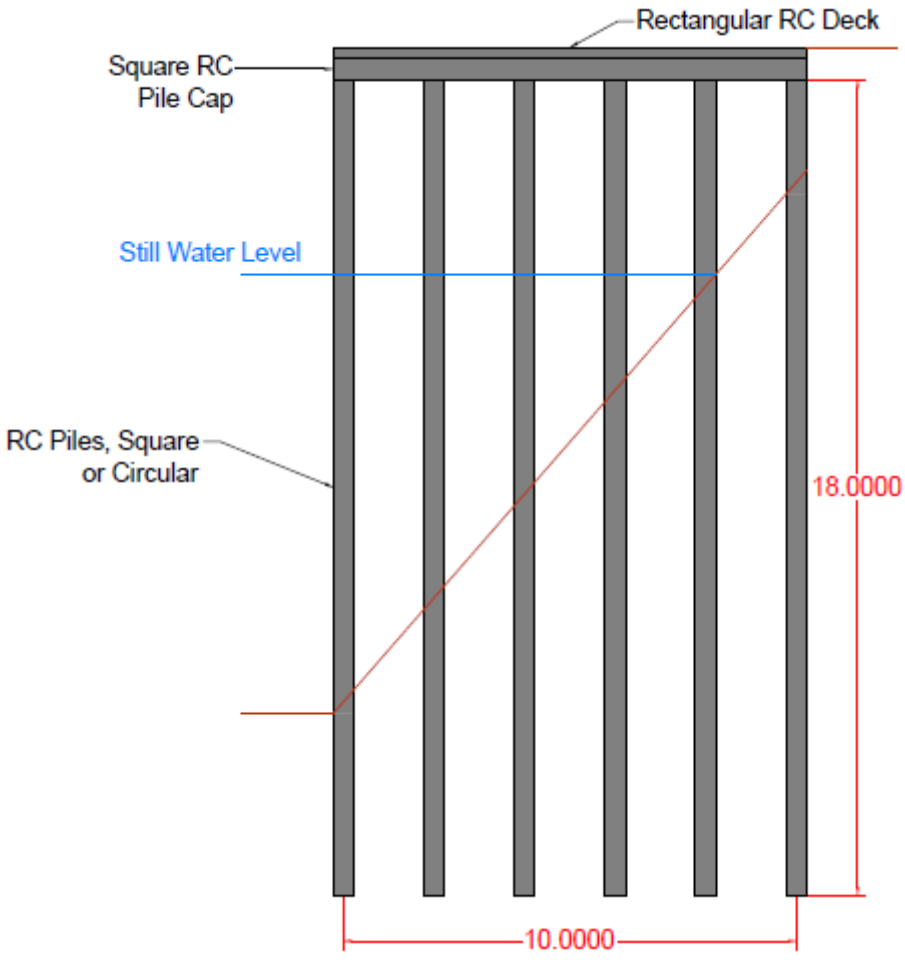

Figure 2: Schematic of base wharf model

Pile types vary from wharf to wharf in New Zealand, though the cross sections used in this study are representative of a range of wharves across New Zealand. Two pile

configurations were tested, one with square piles and one with circular piles. The pile shapes and corresponding sections were the only aspect varied in order to examine the resulting damage to different piles, with the square and circular details based on the database of wharf drawings. The pile cross sections are shown in Figures 3 (a) and (b). The wharf deck also comprises a reinforced concrete section and is shown in Figure 4. The following sections will elaborate upon these model characteristics.

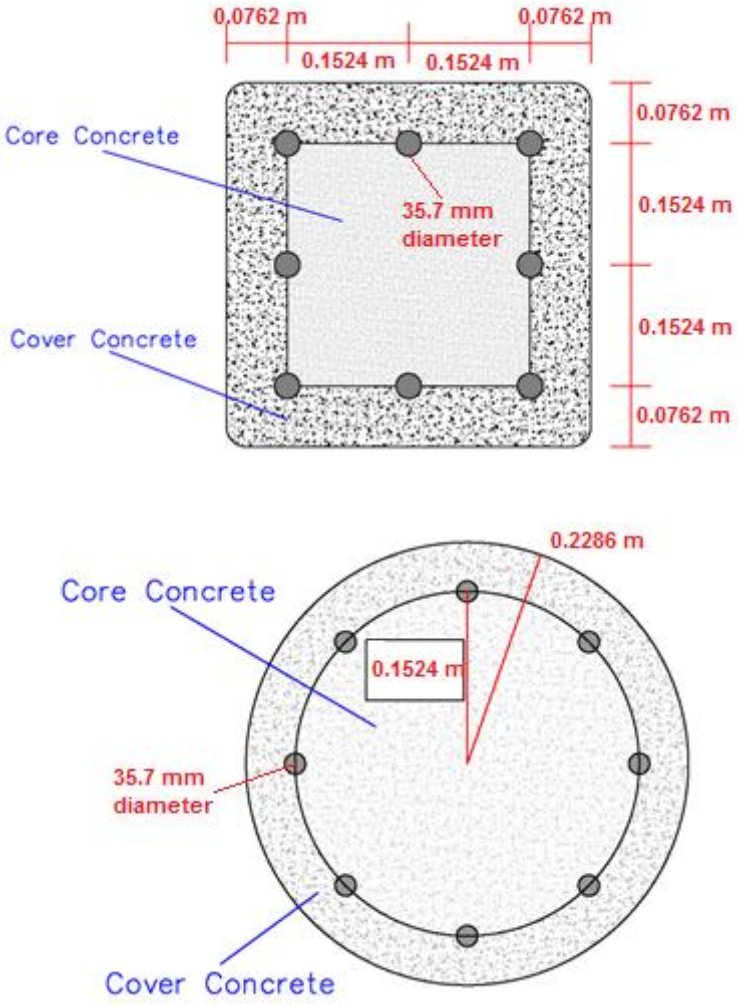

Figure 3: Reinforced concrete pile cross sections tested with base wharf model for (a) square pile and (b) circular pile

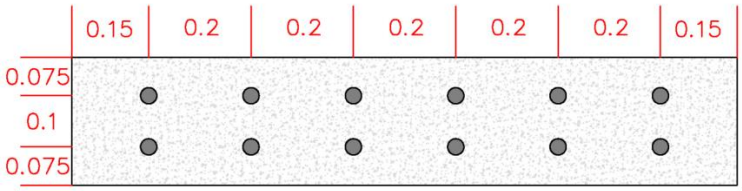

Figure 4: Reinforced concrete deck cross section

3.1 Material Models

The most common material type found in New Zealand wharf structures is reinforced concrete. Reinforcement ratios and cross sections vary between structures and many individual cases are documented. However, the constituent material characteristics are based on typical material properties from construction drawings and typical strengths used during each construction period.

3.1.1 Concrete

The OpenSees concrete model chosen for the purposes of this research was Concrete04: Popovics Concrete Model (Popovics, 1973). This concrete model is characterized by the compressive and tensile response curves shown in Figures 5 and 6.

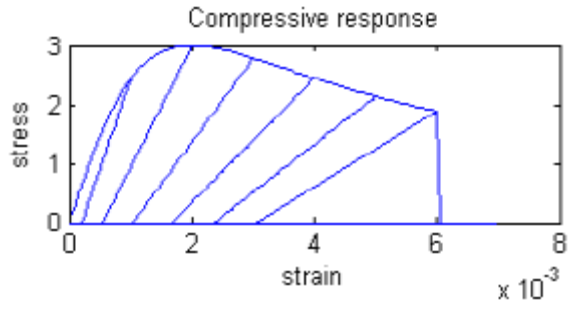

Figure 5: Compressive response curve for Popovics concrete material model

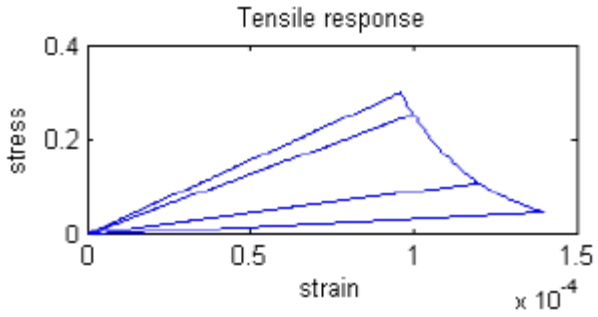

Figure 6: Tensile response curve for Popovics concrete material model

OpenSees requires two separate concrete materials to be developed when modelling a reinforced concrete structure. The first represents cover concrete, the concrete existing outside the bounds of the reinforcement. The second is a core concrete model which represents the concrete under the confining effect of lateral reinforcement. This method is performed in lieu of modelling the lateral reinforcement directly (Mander et al., 1988).

3.1.2 Steel

Rebar was modelled using the Dodd-Restrepo material model. Dodd-Restrepo is a steel model that is designed specifically for rebar in reinforced concrete (Dodd & Restrepo-Posada, 1995). The model includes an initial elastic phase, yield, and strain hardening. The tensile response curve is shown in Figure 7.

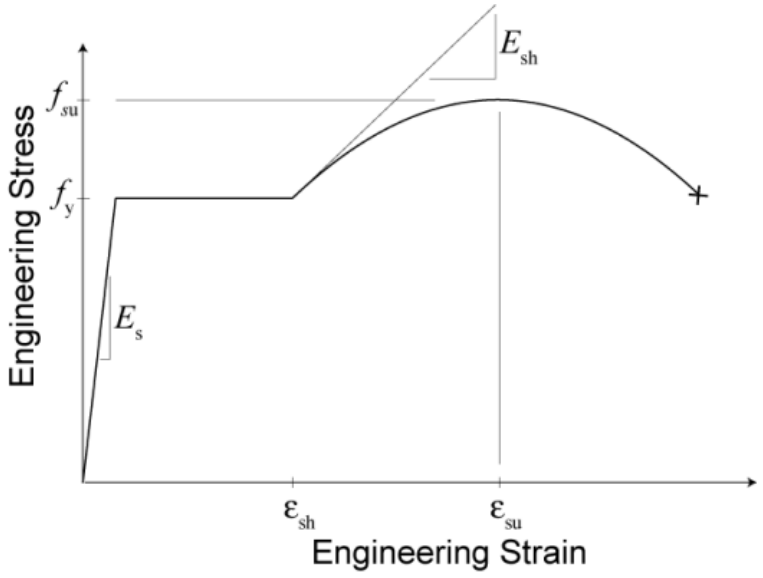

Figure 7: Tensile response curve for Dodd-Restrepo steel model

3.2 Structural Characteristics

3.2.1 Elements

Piles, pile caps, and decks are modelled using either a force (nonlinear) beam-column or a displacement beam-column element. These types of beam-columns consider the spread of plasticity throughout the entire element via a predefined number of integration points along the element's length rather than concentrating deformations at the member's ends. This method of calculating plasticity is shown in Figure 8 (d) which depicts the integration points along the element. The number of integration points used in all analyses was five.

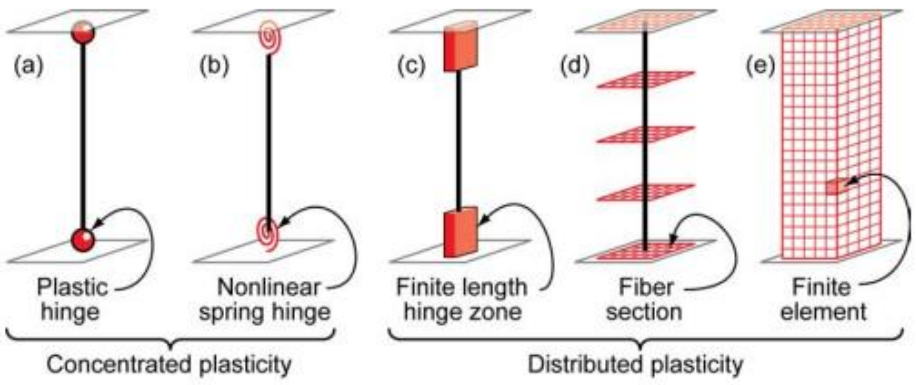

Figure 8: Various methods of modelling plasticity in beam-column elements (Deierlein et al. 2010)

3.2.2 Connections

In wharf design, the connections between members vary in implementation depending on the material of the members. In reinforced concrete piles, the steel rebar typically extends beyond the top end of the pile and directly into the pile cap and deck.

Connections between members (beam-pile and deck-beam connections) were implemented as zero-length members. A zero-length member initially has no length, but is allowed to elongate under stress, resulting in the member deformation. Zero-length members have assigned material characteristics in their x and y directions, which define the stiffness of the element. The resulting member acts as a spring which deforms under loads based on its assigned stiffness.

3.2.3 Soil Model

Pile foundations were represented by zero-length elements with assigned soil stiffness. These zero-length elements connected the pile to an immobile "ground" node. The lateral stiffness of each element was defined by a P-y material which directly relates the force applied to a soil to the lateral displacement. Likewise, vertical resistance was modelled through the use of T-z materials which model skin friction along the length of a pile, and Q-z materials, which model soil bearing at the base of the pile. Implementation of these materials into OpenSees is based on experimentation presented in Boulanger (1999). A visual representation of this application is given in Figure 9.

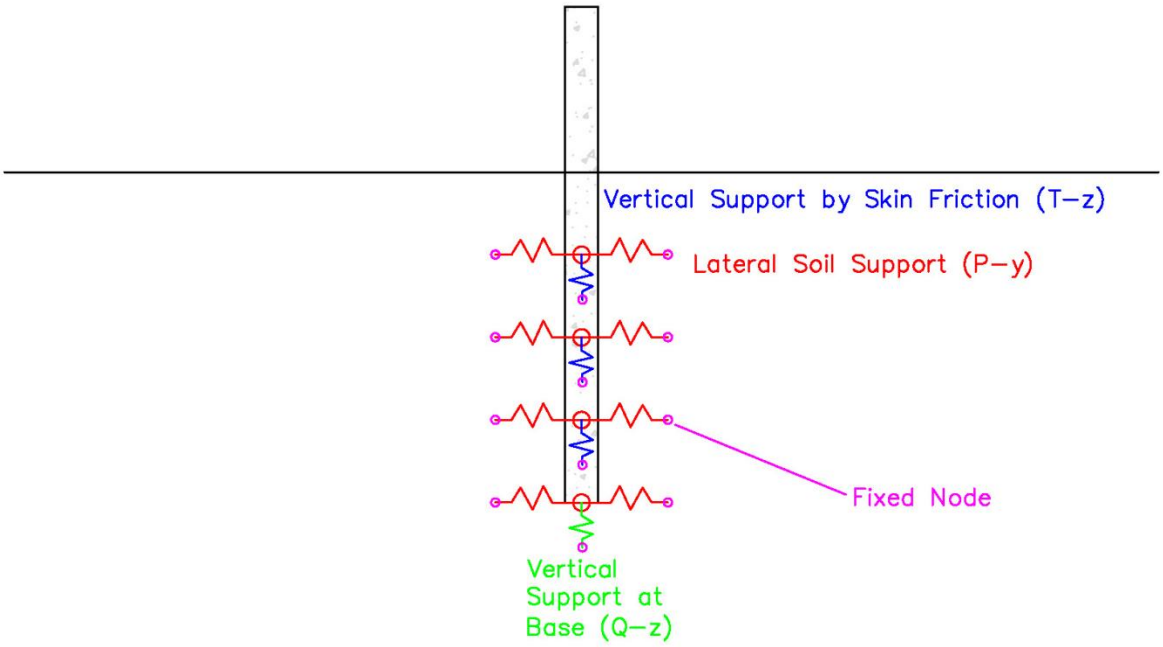

Figure 9: Pile foundation model employing P-y, T-z, and Q-z material models

3.3 Static Loads

Static loads encompass both live and dead loads that, for the purpose of this analysis, are non-variable. This includes structure self-weight, live loads from objects resting on the wharf, lateral hydrostatic loads, and buoyancy.

3.3.1 Self-Weight/Dead Load

Self-weights were based on standard weights of the materials used, 2,400 kg/m^3 for concrete and 8,000 kg/m^3 for steel. These self-weights were applied as distributed loads over the structure. For piles, beams, and girders, the weight was distributed evenly over the length of the entire element.

3.3.2 Buoyancy

Buoyant forces were applied similar to member self-weights, as an upward distributed load along the length of elements. Buoyancy was only applied to submerged sections of elements. The magnitude of the buoyant load is calculated by equation 9.

$$F_B = \rho g V \quad \text{(Eq. 9)}$$

F_B = Buoyant Force

ρ = Density of Water

g = Gravitational Acceleration

V = Volume of Displaced Water

3.3.3 Live Load

A uniform live load of 4.8 kPa was applied directly to the deck member. This was meant to represent objects and facilities that would be located on the wharf deck (POLB, 2012).

3.3.4 Hydrostatic Load

The hydrostatic load on the piles is relevant as it would reduce the magnitude of the tsunami impact on submerged sections. As depth increases, the hydrostatic load increases and thus the impact of the tsunami would be mitigated closer to the seabed. This is not accounted for by applying a hydrostatic load directly to the pile, but rather by reducing the magnitude of the tsunami load below the water surface. At each node where the tsunami load is applied, a load factor is used to define the magnitude with respect to the time series. A load factor of 1.0 applies the full load whereas a load factor of 0.5 applies only half the magnitude. The load factor was reduced for each node based on the depth and by extension,

the hydrostatic load present as a percentage of the total tsunami load. Nodes located above the still water level were invariably assigned a load factor of 1.0.

3.4 Application of Tsunami Loads

Due to the discrepancy in the number of studies quantifying lateral and uplift hydrodynamic loads respectively, the lateral tsunami loads applied to the structural model were based on the design code-based loads. Uplift loads were based on a combination of design code data and the tsunami wave flume studies carried out at the University of Auckland, with the main thrust coming from the latter.

Tsunami loads were applied in terms of a number of time series**.** The wharf structure comprised several elements connected by nodes. At each node, a tsunami load time series was applied that consisted of both an initial peak impact and a sustained steady-state load. The initial impact was first applied to the nodes farthest over the water, where the tsunami would theoretically strike first (assuming it approached perpendicularly). At those first nodes, the initial impact gave way to the steady-state load as the tsunami progressed. The same time series was applied to the rest of the structure, but was staggered to begin at a later time step to account for the travel time to each node. This stagger was based on the theoretical velocity of the tsunami and the distance between the nodes. This setup was chosen as a result of the short duration of the tsunami's initial impact and the difficulty in achieving convergence at larger step sizes. The result was a theoretical ten second duration of structure inundation which provided enough time for the entire structure to reach a steady-state stress distribution. As both the lateral and vertical loads consist of impact and steady-state phases, similar procedures were used in their developments. The progression of the tsunami time series can be seen in Figure 10.

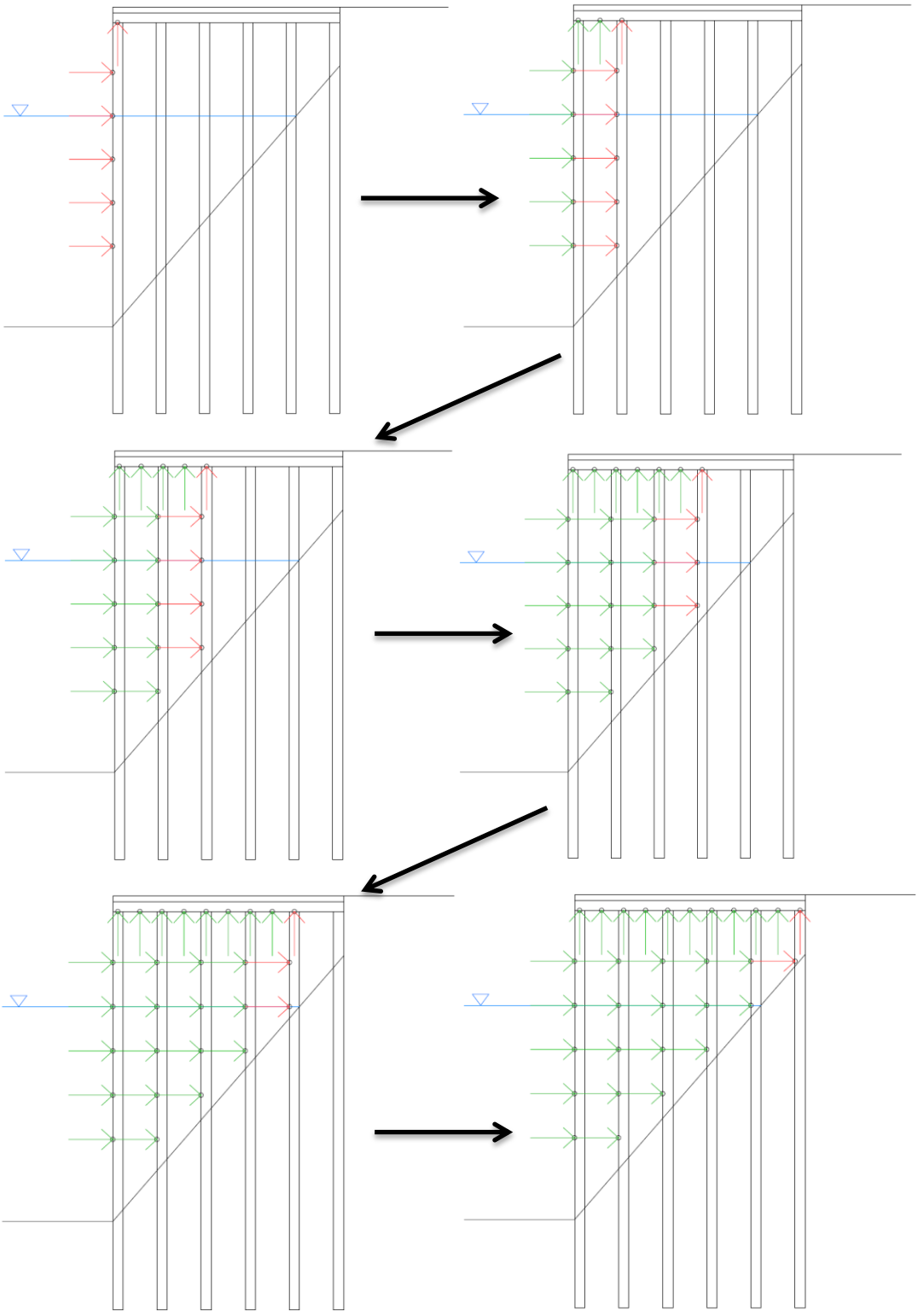

Figure 10: Progression of tsunami loading time series. Red arrows indicate initial impact while green represent steady-state hydrodynamic load.

As discussed in section 2.3, there was good agreement between the uplift load magnitudes derived from the design standards and those quantified experimentally. In the experimentation, the initial impact of the tsunami uplift was found to average 1.9 times the steady-state magnitude with little variation between relevant tests. Lateral hydrodynamic loads were calculated through design standards. Since more experimentation has been carried out in attempts to quantify lateral tsunami loads, these approximations were said to be more reliable and thus no additional experimentation was attempted. Design standards featured equations for both wave slam and lateral hydrodynamic loading, providing values for both phases of the time series.

Chapter 4: Results

Stresses that were recorded throughout the wharf structures during the analysis were ultimately used to assign damage states. Recorders were placed along the lengths of all members to attain stresses at several points, granting a more comprehensive vision of the stress distribution and better damage state estimates. The following sections summarise the damage characteristics and the representation of overall structural damage with increasing bore height.

4.1 Tensile Stresses

Axial tension throughout the structure was the controlling internal force component in most analyses. The nature of the load patterns left most of the structure in tension, with the exception of the deck and pile cap. The compressive forces in these members were not high enough to put either the concrete or reinforcement in danger of failing. Tension controlled each defined damage state for the purposes of this analysis. In order to assess the locations of high stresses, and thereby the locations where significant damage would be expected, the tensile stresses were recorded for each element. The maximum tensile stress in each element was then plotted as a percentage of the yield stress of the steel rebar. Note that the focus of this research was on above ground elements to which the loads were directly applied. The results for a four and ten metre tsunami are shown in Figures 11 (a), (b), (c), and (d).

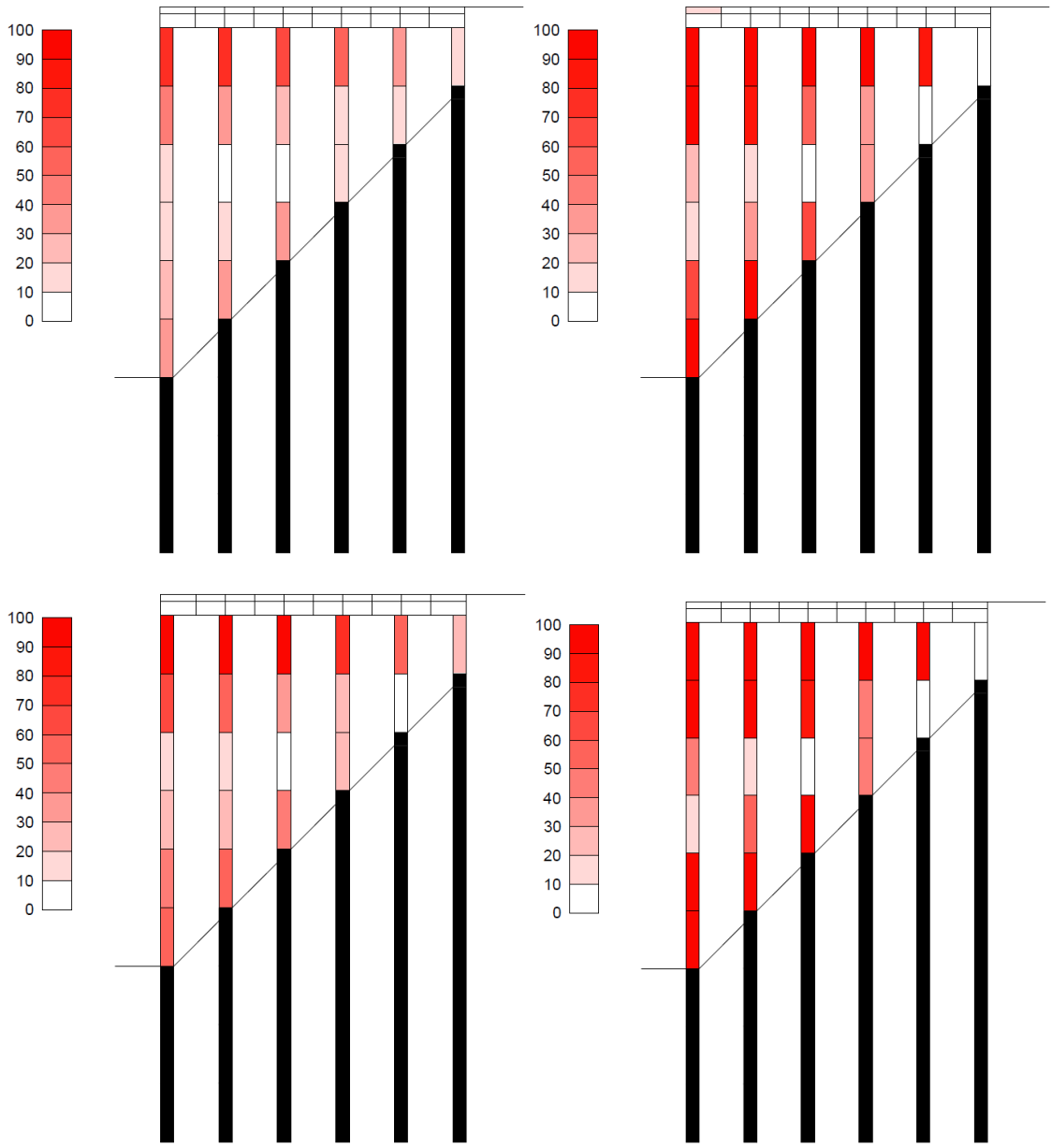

Figure 11: Tensile stress in each wharf element as a percentage of yield strength of steel for (a) square piles under four metre tsunami (top left), (b) square piles under ten metre tsunami (top right), (c) circular piles under four metre tsunami (bottom left), and (d) circular piles under ten metre tsunami (bottom right).

The highest tensile stresses are concentrated at the tops and bottoms of the piles. The decks and pile caps experience very little tensile stress. As the lateral load causes the piles to deflect towards the shore, this component of the load likely induces compressive stresses in the horizontal members which would balance the tension from uplift to some degree. Conversely, both the uplift and the lateral loads induce tensile stresses in the piles which results in extensive damage.

4.2 Shear Stresses

Maximum shear stress was initially collected in addition to tensile stresses and figures were generated to depict potential sections of the wharf that would suffer from shear cracking. It was assumed that this play a role in structural damage states as a result of high magnitude loads impacting the structure perpendicularly to the members. However, it quickly became clear that shear stresses were significantly less than the section capacities. Thus shear stress was not a controlling failure mode.

4.3 Damage States

Initially, the goal was to develop fragility models which would relate the probability of damage to a structure to the wave height of the tsunami. However, basing this analysis on computational models alone is difficult as the OpenSees model will produce the same result each time it is run. Thus a probability of damage cannot be developed. Rather than define a probability of damage occurring to a structure, a series of damage states was defined. Each structure was tested at several wave heights and the resulting damage state of each member was isolated. The state of the overall structure was then assessed based on the number of members that fell within each damage state. The various damage states are as follows:

1. Elastic – An element falling within the elastic state has not surpassed the elastic phase on the stress-strain curve. Thus when the load is removed, the element will return to its original state with no permanent damage. Concrete within the elastic state has not cracked and steel has not reached its yield point.

2. Cracked – Applies to concrete which in which the tensile stress has exceeded the modulus of rupture, thus resulting in tensile cracking. The damage state is assessed by examining the stresses at the edges of the element cross sections. As the modulus

of rupture is simply a function of the concrete compressive strength, it can easily be calculated and compared to the internal stress. A member generally reaches the point of cracking long before yield.

3. Yield – Applies to steel when the internal tensile stress in the rebar exceeds the yield strength. This damage state is assessed by recording the stresses at the locations of the rebar within the cross section and comparing to the steel's defined yield strength.

4. Fracture – Applies to steel when the rebar tensile stress exceeds the ultimate tensile strength (UTS), causing the steel to fracture completely. Like yield, this is detected by recording the stress at the locations of the rebar and comparing to the UTS which is defined as a material property of the steel model.

The overall damage state of the wharf was assessed by assigning these four damage states to members. This analysis resulted in a series of figures indicating the resulting damage state of each structural element. Presented here in Figures 12 (a), (b), (c), and (d) is the resulting damage states generated by the minimum and maximum wave heights tested, four and ten metres.

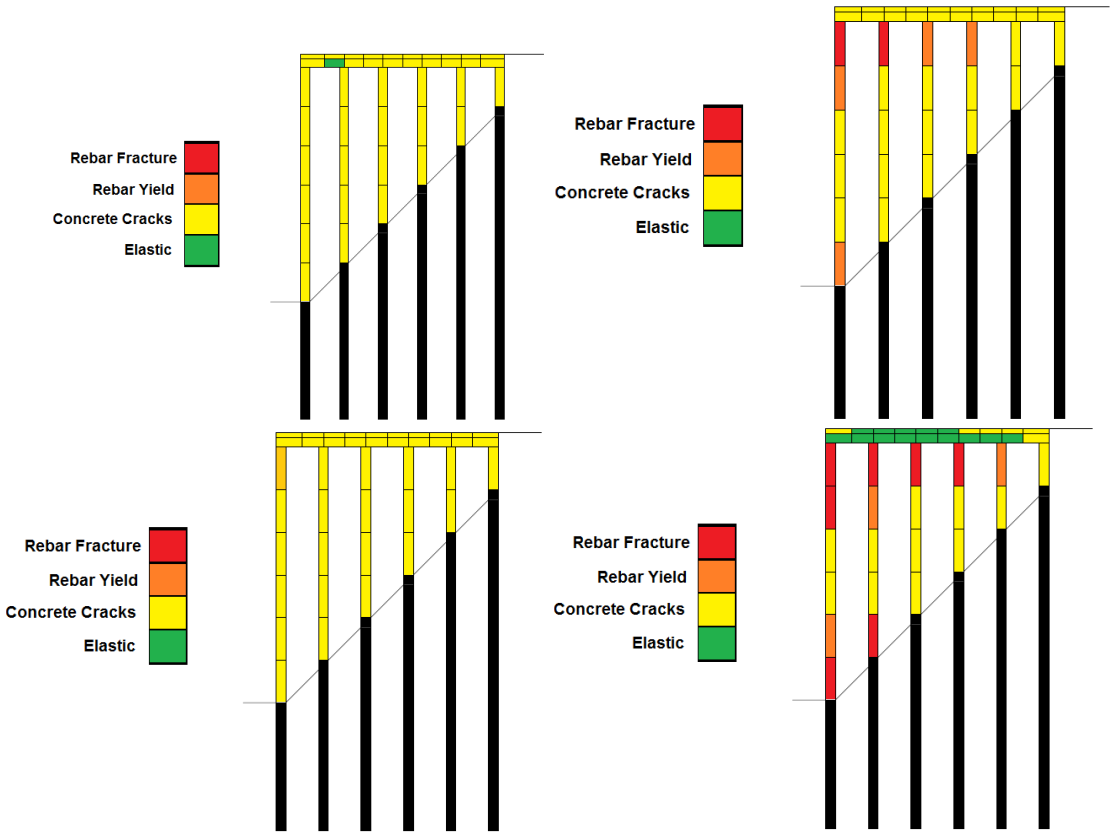

Figure 12: Damage state of each constituent element for (a) square piles under four metre tsunami (top left), (b) square piles under ten metre tsunami (top right), (c) circular piles under four metre tsunami (bottom left), and (d) circular piles under ten metre tsunami (bottom right).

The results indicated that the damage was largely concentrated in the piles. In no analysis did the deck or pile cap elements reach yield or fracture. Therefore, when evaluating and comparing the resulting damage states, the piles were the main focus. The overall damage state was quantified by collectively examining the elements each pile, then assigning a damage value to the member. In each case, the damage state of the member was defined by the most severely damaged element. For example, if one element fractured in a pile while the remainder cracked, the pile was considered fractured. This is justified as the pile would likely need to be replaced regardless of the extent of the fracture.

Once each pile's damage state was determined, the damage states were assigned corresponding values between 0 and 1. These values are summarised in Table 2.

Table 2: Damage states and associated levels

Damage State	Level
Elastic	0
Cracking	0.33
Yield	0.66
Fracture	1.0

The damage level of each pile was then averaged to produce an overall damage state for the wharf. This allowed for a quantifiable comparison of the damage extents of each wharf under each tsunami magnitude. The results of this analysis are presented in Figure 13.

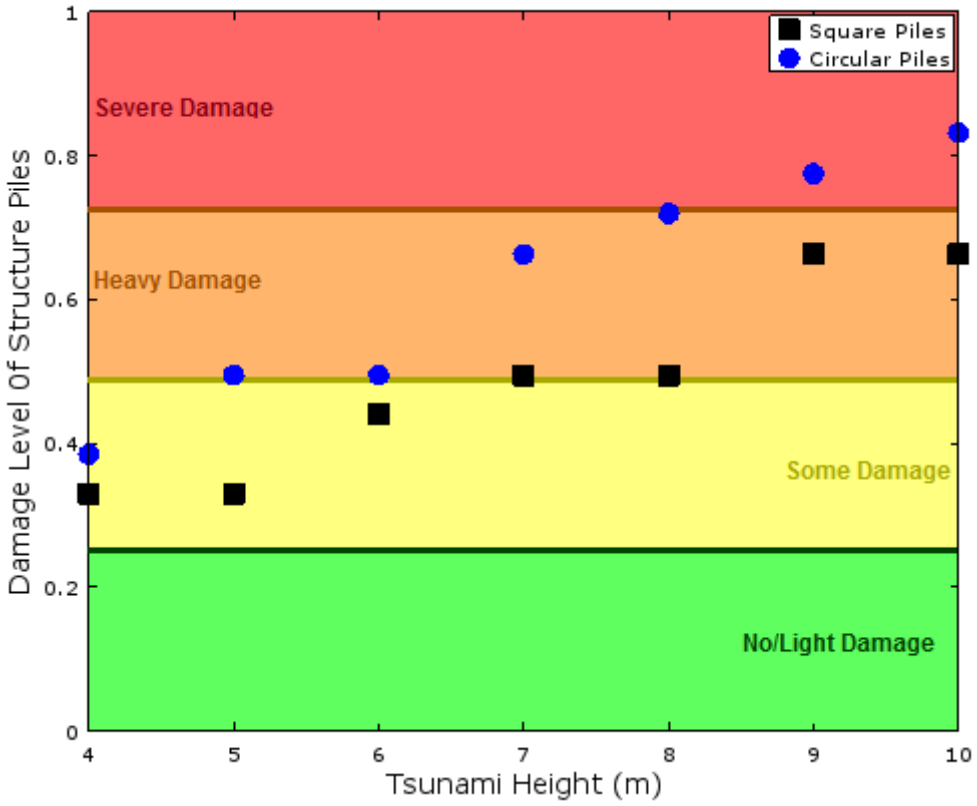

Figure 13: Comprehensive damage states of wharf structures under loading from given tsunami height

Although the reinforcing ratio is higher for the circular pile (as a result of a smaller cross section), the damage states to a wharf with circular piles were more severe than those to an equivalent wharf with square piles. In order to reduce the damage to equivalent levels of the square piles, the reinforcing ratio would need to be increased which would likely introduce additional costs.

It should be noted that fracture of a pile will not necessarily render the entire wharf structure unusable, though it will weaken it substantially. Depending on the geometry, the live loads, and the duration of tsunami loading beyond initial pile fracture, the wharf may be serviceable as a whole if one pile is destroyed. In most cases, more than one fractured pile would likely result in severe damage to the wharf and compromise its structural stability.

Chapter 5: Conclusions

This work was carried out in several stages. The first stage was to quantify tsunami loads. As there is significant research available related to lateral tsunami loads, no additional laboratory testing was deemed necessary. Hydrodynamic uplift has received much less attention. Two concurrent studies were carried out to quantify tsunami uplift as modelled by a tsunami bore and a solitary wave. The results of these studies revealed that uplift from a solitary wave is lower in magnitude that from a tsunami bore. Additionally, the tsunami bore loads closely resembled those predicted in *Guidelines for the Design of Structures for Vertical Evacuation from Tsunami* (FEMA, 2008). Thus the bore loads were deemed more reliable for the purpose of applying to the structural model. The loads characterised by the solitary wave study still produced results which may be useful in other applications, such as storm surge studies.

The second phase of this work sought to predict damage states to representative structural wharf models that resembled existing infrastructure in New Zealand ports. A base wharf model was developed and the piles were changed to accommodate two different possible configurations. The geometry, materials, and structure of the model bore resemblance to existing port infrastructure in New Zealand. The quantified tsunami loads were compiled into time series based on the approaching wave height. The time series, consisting of both tsunami initial impact and steady state phases, were then applied to the structural models. The resulting stresses in each member were recorded and the damage states were plotted.

While all wave heights tested generated some damage to the structure, there was a clear increase in damage as the tsunami wave height increased. Many of the tests resulted in stresses that exceeded the yield strength of the reinforcing steel. Nine and ten metre wave

heights caused complete fracture of one or more piles. The wharf supported by circular piles consistently resulted in a more severe damage state than an equivalent structure with square piles.

5.1 Future Work

In addition to the damage states calculated, this research has laid the groundwork for future studies. Knowledge and research related to tsunami loads is constantly expanding and while some sectors remain in early stages, every step taken adds to the knowledge base. However, this will be followed up with applications of those tsunami loads to design standards and other studies predicting structural damage. In large part, existing research related to fragility models is developed from field observation following tsunami. It is important to observe, but an improved ability to predict will potentially mitigate impact.

In the immediate future, more wharf layouts will be tested. As the results of this study are restricted in use to the specific type of wharf tested, a greater breadth of geometric layouts, material strengths and properties, soil properties, structural member types, and other characteristics must be implemented and tested. Further, experimentation over a larger range of bore heights and velocities are necessary as well as better ways of applying these loads to structural models. These are issues that will be examined further in future modelling.

Works Cited

Bormann, P. (2008). *Tsunami Information Sheet*. Helmholtz Centre Potsdam: GFZ German Research Centre for Geosciences.

Boulanger, R. W., Curras, C. J., Kutter, B. L., Wilson, D. W., & Abghari, A. (1999). Seismic Soil-Pile-Structure Interaction Experiments and Analysis. *Journal of Geotechnical and Geoenvironmental Engineering, 125*(9), 750-759.

CCH. (2000). City and Council of Honolulu Building Code. In: Department of Planning and Permitting of Honolulu Hawaii.

Chen, C., Melville, B., Shafiei, S., Popovich, B., Shamseldin, A., & Wotherspoon, L. (2015). Quantifying Uplift Loads on Pile Supported Wharf Structures, Part 1: Tsunami Bore. *Coasts and Ports Conference 2015*. Auckland, New Zealand, 15-18 September 2015.

Chen, C., Melville, B., Nandasena, N., Shamseldin, A., & Wotherspoon, L. (2016). Experimental Study of Uplift Loads Due to Tsunami Bore Impact on a Wharf Model. Submitted to *Coastal Engineering*.

Deierlein, G., Reinhorn, A., & Willford, M. (2010). *Nonlinear Structural Analysis for Seismic Design: A Guide for Practicing Engineers*. (NIST GCR 10-917-5). National Institute of Standards and Technology.

Dodd, L. L. & Restrepo-Posada, J. I. (1995). Model for Predicting Cyclic Behaviour of Reinforcing Steel. *ASCE Journal of Structural Engineering*, 121(3), 433-445.

FEMA. (2008). Guidelines for the Design of Structures for Vertical Evacuation from Tsunamis: Federal Emergency Management Agency.

FEMA. (2011). *Coastal Construction Manual* (Fourth ed.): Federal Emergency Management Agency.

Kosa, K., Nii, S., Miyahara, K., & Shoji, M. (2011). Experimental Study for Estimating Tsunami Forces Acting on Bridge Girders. *Proceedings of JSCE*.

Mander, J., Priestley, M., & Park, R. (1988). Theoretical Stress-Strain Model for Confined Concrete. *Journal of Structural Engineering*, 114(8), 1804-1826.

Palermo, D. (2008). Tsunami-Induced Loading on Structures. *Structure Magazine*, *2008*(March), 10-13.

POLB. (2012). Port of Long Beach Wharf Design Criteria, V 3.0: Port of Long Beach.

Popovich, B., Wotherspoon, L., Shafiei, S., Chen,C., Melville, B., & Shamseldin, A. (2015). Quantifying Uplift Loads on Pile Supported Wharf Structures, Part 2: Solitary Wave. *Coasts and Ports Conference 2015*. Auckland, New Zealand, 15-18 September 2015.

Popovics, S. (1973). A Numerical Approach to the Complete Stress-Strain Curve of Concrete. *Cement and Concrete Research, 3*, 583-599.

Shafiei, S., Melville, B., Shamseldin, A., Watts, M., & Hoffman, T. (2015). Experimental Investigation of Tsunami Bore Induced Scour Around Structures. *Coasts and Ports Conference 2015*. Auckland, New Zealand, 15-18 September 2015.

Shafiei S., Melville B.W., Beskhyroun S. and Shamseldin A.Y. (2014). Preliminary Investigation of the Tsunami-Borne Debris Impact on Structures: A new method for impact force measurement. 5th International Symposium on Hydraulic Structures, Brisbane, Australia, 25-27 June 2014.

Statistics NZ. (2012). Infoshare: Statistics New Zealand. from http://www.stats.govt.nz/infoshare/